

## 19. SITE 854<sup>1</sup>

### Shipboard Scientific Party<sup>2</sup>

#### HOLE 854A

**Date occupied:** 27 June 1991  
**Date departed:** 28 June 1991  
**Time on hole:** 9 hr, 40 min  
**Position:** 11°13.433'N, 109°35.652'W  
**Bottom felt (rig floor; m; drill-pipe measurement):** 3579.6  
**Distance between rig floor and sea level (m):** 11.7  
**Water depth (drill-pipe measurement from sea level, m):** 3567.9  
**Total depth (rig floor; m):** 3626.4  
**Penetration (m):** 46.8  
**Number of cores (including cores with no recovery):** 3  
**Total length of cored section (m):** 28.70  
**Total core recovered (m):** 20.89  
**Core recovery (%):** 72.8  
**Oldest sediment cored:**  
Depth (mbsf): 28.7  
Nature: zeolitic Fe-oxide clay  
Earliest age: late Miocene  
**Drill below core(m):** 18.1

#### HOLE 854B

**Date occupied:** 28 June 1991  
**Date departed:** 28 June 1991  
**Time on hole:** 4 hr, 46 min  
**Position:** 11°13.433'N, 109°35.652'W  
**Bottom felt (rig floor; m; drill-pipe measurement):** 3579.1  
**Distance between rig floor and sea level (m):** 11.7  
**Water depth (drill-pipe measurement from sea level, m):** 3567.4  
**Total depth (rig floor; m):** 3624.5  
**Penetration (m):** 45.4  
**Number of cores (including cores with no recovery):** 5  
**Total length of cored section (m):** 45.4  
**Total core recovered (m):** 48.01  
**Core recovery (%):** 105.7  
**Oldest sediment cored:**  
Depth (mbsf): 45.4  
Nature: clayey metalliferous sediments  
Earliest age: late Miocene

#### HOLE 854C

**Date occupied:** 28 June 1991  
**Date departed:** 29 June 1991  
**Time on hole:** 18 hr, 19 min  
**Position:** 11°13.431'N, 109°35.649'W  
**Bottom felt (rig floor; m; drill-pipe measurement):** 3579.9  
**Distance between rig floor and sea level (m):** 11.70  
**Water depth (drill-pipe measurement from sea level, m):** 3568.2  
**Total depth (rig floor; m):** 3625.9  
**Penetration (m):** 46.0  
**Number of cores (including cores with no recovery):** 6  
**Total length of cored section (m):** 46.0  
**Total core recovered (m):** 54.03  
**Core recovery (%):** 117.5  
**Oldest sediment cored:**  
Depth (mbsf): 46.00  
Nature: clayey metalliferous  
Earliest age: late Miocene

**Principal Results:** Site 854 (WEQ-2) is the northernmost site of the Leg 138 north-south transect along 110°W. This was one of the alternative sites in the Leg 138 prospectus, and because of the time gained during the cruise, we were able to add it to the leg. The site is presently located within the westward-flowing North Equatorial Current (NEC) in an area of relatively thin sediment cover. The objective of drilling at the site was to provide a record of eolian sedimentation in a region influenced by Northern Hemisphere trade-wind circulation with minimal direct influence of the Southern Hemisphere trade winds.

Three holes were drilled at Site 854. Because of the thin sediment cover and limited time available to complete the site, Hole 854A was first APC-cored to 19.4 mbsf. To prevent damaging the APC core by striking basement and possibly forcing a trip through the pipe, we tried to retrieve a single XCB core, and then Hole 854A was drilled to basement at 46.8 mbsf. This depth was in close agreement with an estimate based on the 3.5-kHz records collected during the pre-site survey. Holes 854B and 854C were then APC-cored to 45.4 and 46.0 mbsf, respectively.

The dominant lithologic components in the 46 m sedimentary sequence are clay, nannofossils, foraminifers, and metalliferous oxides. The upper 22 m consists of alternating foraminifer ooze, nannofossil ooze, and clay. Between 22 and 32 mbsf, the sediment is a more homogeneous oxide-rich clay having lesser amounts of nannofossils and minor amounts of zeolites. Nannofossil content again increases in the interval between 32 to 38 mbsf. Below 39 mbsf, black metalliferous clay and clayey metalliferous sediments high in iron and manganese oxide were recovered. These black metalliferous sediments were not recovered at any of the previous sites.

All major fossil groups were found in the upper Pliocene and Pleistocene section of the site. With the exception of foraminifers, which exhibit poor preservation, the chief microfossil groups exhibit moderate to good preservation. Calcareous nannofossils indicate a possible hiatus marked

<sup>1</sup> Mayer, L., Pisias, N., Janecek, T., et al., 1992. *Proc. ODP, Init. Repts.*, 138: College Station, TX (Ocean Drilling Program).

<sup>2</sup> Shipboard Scientific Party is as given in list of participants preceding the contents.

by a Mn-rich "hard ground" layer and extending over nannofossil zones CN12–CN9b. Below this possible hiatus, foraminifers and siliceous microfossils are generally absent, and calcareous nannofossils are generally poorly preserved.

Magnetic remanence is stable throughout the entire section. Even though the multishot camera could not be used in this shallow site, the continuously recovered section in the three holes, together with a stable inclination pattern, permitted reasonably unambiguous polarity selections. Nannofossils and radiolarians in the upper 19 m and nannofossils in the lower section provide sufficient time control to constrain the magnetostratigraphic sequence absolutely. Above a possible hiatus, all magnetic events spanning the Brunhes to the base of the Gauss could be identified. Below this hiatus, all magnetic events from the top of Chron C3A to the top of Chron C5 were identified.

The excellent magnetostratigraphy allows for a detailed set of sedimentation rate estimates for Site 854. As expected from the thin sediment cover, sedimentation rates are low and average ~5 m/m.y. from ~0 to 3 Ma. The interval between 3.5 and 5.3 Ma is one of very reduced sedimentation and may prove to be the first hiatus detected during Leg 138. Sedimentation rates were highest during the interval of 6.5 to ~7.5 Ma, reaching values of ~15 m/m.y. The basal metalliferous sediments accumulated at rates of ~5 m/m.y.

Site 854 was the last site drilled during Leg 138. The site brought the total amount of recovery of the leg to an ODP record of 5536.8 m, with an average core recovery of 99.9%. At the conclusion of the leg, we had collected 7155 m of log records in 153 hr of logging, travelled 5415 nmi, and thus accumulated a record total of 9.15 log (m<sup>2</sup>kt). We hope that all future ODP legs can better this record.

## BACKGROUND AND SCIENTIFIC OBJECTIVES

Site 854, the last site of Leg 138, is the northernmost site of our 110°W, north-south transect. The site lies beneath the westward-flowing North Equatorial Current (Fig. 1) and is located on thinly sedimented crust ~9 m.y. in age. The site lies on the Pacific Plate, which has a well-defined backtrack history (Fig. 2), although several poles of rotation have been suggested (Duncan and Clague, 1985; van Andel et al., 1975). Our primary objective for drilling at the site was to provide a record of eolian transport associated with the Northern Hemisphere trade winds in an area minimally influenced by Southern Hemisphere atmospheric circulation.

Because sediment in the region is so thin, we found it difficult to select a site. The initial site survey during the Venture 1 cruise of the *Thomas Washington* located a region having relatively minor topographic relief and several potential sedimentary targets (Fig. 3). The site survey area lies south of a large region of very rough topography and little sediment and just north of the Clipperton Fracture Zone. The true thickness of the sediment was generally too thin for adequate resolution with the *Thomas Washington's* water-gun system (Fig. 4) and, thus, a careful 3.5-kHz survey was conducted before beacon deployment. The site is situated on a broad, gently sloping, north-south-trending high. The sediment cover on this high is thin and varies in thickness from a few meters to >40 m. The site was selected in a small depression that may have acted as a sediment trap (Fig. 5). The sediment thickness at this site was estimated as ~45 m, based on the 3.5-kHz records.

## OPERATIONS

### Transit to Site 854

The transit to Site 854 covered 236 nmi and averaged 10.5 kt. Upon reaching the proximity of the site at 2115L (all times reported in operations text are local time, L, where local time is Universal Time Coordinated, UTC, minus 7 hr; all times in Table 1 are UTC) 27 June, the vessel slowed to 6 kt for conducting a site survey with the 3.5-kHz echo sounder. At 2315L, a beacon was deployed, after which the ship came about and returned to the site location by 2330L. The survey

covered 13 nmi at an average speed of 5.9 kt. The depth to seafloor, based upon the precision depth recorder (PDR), was 3584.0 below the rig floor (mbrf).

### Hole 854A

The drill pipe was lowered to 3580 mbrf, and the first piston core was retrieved at 0545L 28 June; from it we recovered 9.96 m of sediment (see Table 1 for a summary of coring operations). The first core established the mud line at 3579.1 mbrf. Only one more APC core was recovered from this hole (Core 138-854A-2H, 9.9–19.4 mbsf). With such a thin sedimentary section providing little lateral stability for the bottom-hole assembly (BHA), we were concerned that were the piston core to impact the basalt in such conditions, the piston rod might get bent. Should that happen, the core barrel would have had to be retrieved with a trip through the pipe. Because of time constraints at this last site, we could not have accommodated an extra pipe-trip and still attain our site objectives. Thus, the XCB-coring system was used to retrieve the next core. When Core 138-854A-3X was recovered with only 0.96 m of sediment (in sediment too soft for the XCB), we decided to advance ahead by drilling and define the basement depth. Basement was reached at 46.8 mbsf by 0800L. The pipe was then pulled out of the hole, and the bit cleared the mud line by 0855L, ending Hole 854A.

### Hole 854B

Without offsetting the ship, Core 138-854B-1H was taken at 0950L 28 June, in a water depth of 3578 mbrf; from it we recovered 8.38 m of sediment, establishing the mud-line depth at 3579.1 mbrf. Piston-coring advanced quickly to 45.4 mbsf (Core 138-854B-5H), and we recovered 48.01 m of sediment (105.7% recovery). After Core 138-854B-5H was brought on deck, the pipe was pulled out of the hole, and the bit cleared the mud line at 1341L 28 June, thereby ending the hole.

### Hole 854C

Hole 854C was the 42nd hole and the last one drilled during Leg 138. The last mud-line core was retrieved in a water depth of 3574 mbrf at 1445L 28 June, and from it, we recovered 3.6 m of sediment to establish the mud line at 3579.9 mbrf. Piston-coring advanced to 46.0 mbsf, and we recovered 54.03 m of sediment (117.5% recovery). (With the recovery of Core 138-854C-3H, the old ODP recovery record of 5502 m, set during Leg 133, was broken.) The last core in the hole (Core 138-854C-6H) was advanced only 4.4 m to avoid hitting basement and to attempt to recover as much of the section above basement as possible. The retrieved core barrel contained 10.11 m of sediment. The drill bit apparently moved laterally since this core showed no visible signs of disturbance. After Core 138-854C-6H was recovered, we pulled the pipe out of the hole and brought the bit on deck at 0410L 29 June.

## Transit to San Diego

The vessel was under way at full speed toward San Diego at 0800L 29 June. The *JOIDES Resolution* arrived at the dock in San Diego at 1530L, 4 July 1991.

## LITHOSTRATIGRAPHY

### Introduction

Three holes were drilled at Site 854 to recover a 46 m sequence of Pleistocene to upper Miocene (0–8.92 Ma) sediments (Figs. 6 and 7). The dominant lithologic components are clay, nannofossils, foraminifers, and oxides. The uppermost 22 m consists of alternating foraminifer ooze, nannofossil ooze, and clay having variable quanti-

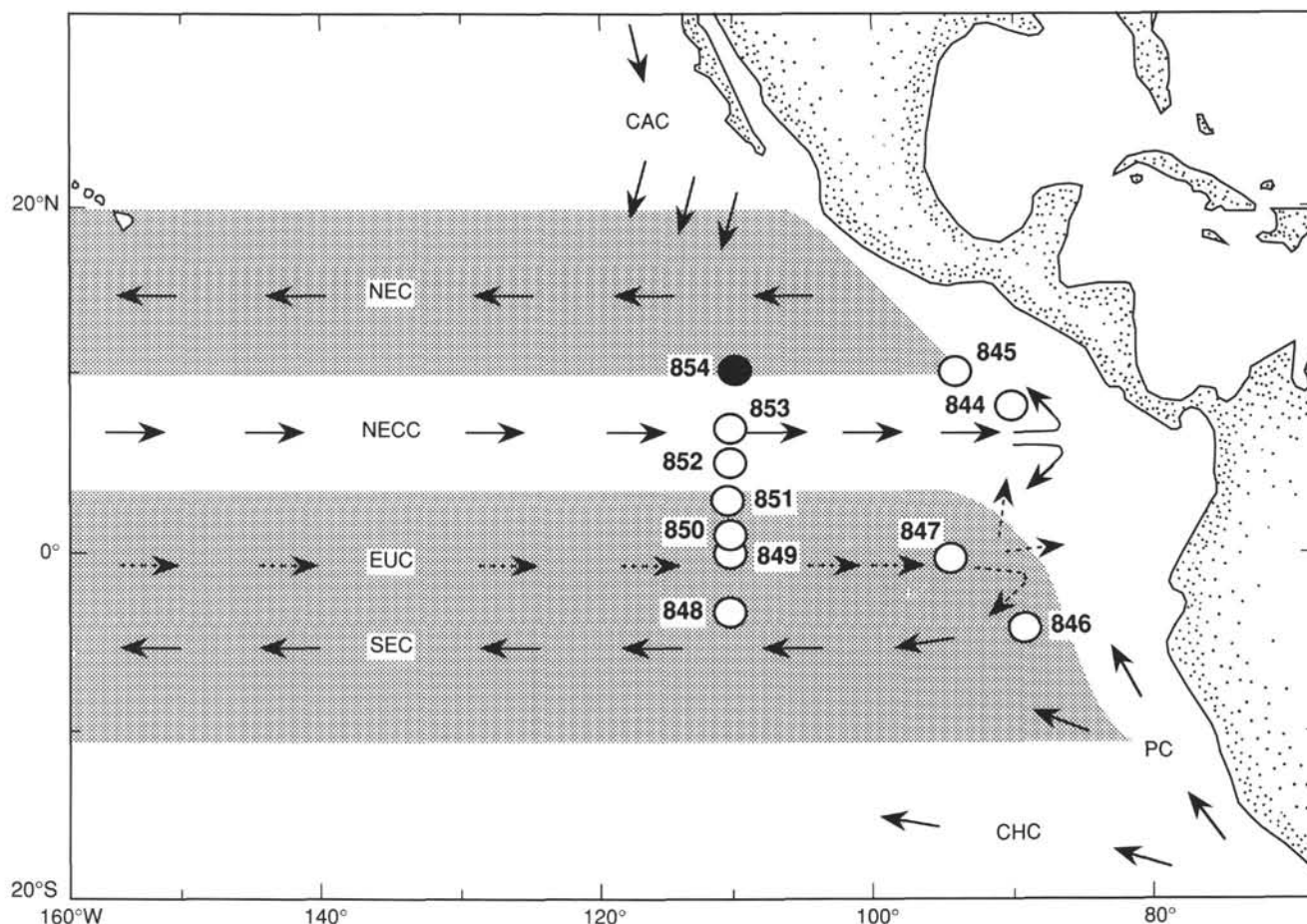


Figure 1. Location of Site 854 and generalized circulation system of the eastern equatorial Pacific Ocean. Other Leg 138 sites are shown for reference. Surface current shown as solid arrows, sub-surface current as dashed arrows. CAC = California Current; NEC = North Equatorial Current; NECC = North Equatorial Countercurrent; EUC = Equatorial Undercurrent; SEC = South Equatorial Current; PC = Peru Current; and CHC = Chile Current. Shaded area illustrates general latitudinal extent of the SEC and NEC.

ties of the major components and of diatoms and radiolarians. Between ~22 and 32 mbsf, a more homogeneous oxide-rich clay containing lesser amounts of nannofossils and minor zeolites is the dominant lithology. The nannofossil content of the sediment increases between 32 and 38 mbsf, but clay and oxides are the only other significant components. Below ~39 mbsf, black metalliferous clay and clayey metalliferous sediments containing extremely high iron and manganese oxide concentrations were recovered.

### Description of Lithology

#### Lithologic Unit I

##### Intervals:

Cores 138-854A-1H through -3X

Cores 138-854B-1H through -5H

Cores 138-854C-1H through 6H

Age: Pleistocene to late Miocene, 0–8.92 Ma

Depth: 0–20.9 mbsf, Hole 854A; 0–48.0 mbsf, Hole 854B; 0–54.0 mbsf, Hole 854C

Sediments in the uppermost 22 mbsf (25 mcd) of Site 854 alternate among several lithologies. Clay, foraminifers, and nannofossils are the predominant lithologic components, each representing up to 60% of the sediment in specific beds (Fig. 8). Diatoms, radiolarians, and

Fe- and Mn-oxides are also present, but are less abundant. Slow sedimentation rates (see "Sedimentation Rates" section, this chapter) and intense bioturbation have resulted in gradual transitions between the major lithologies. Sediment color is generally pale brown to dark yellowish-brown (10YR 6/3–10YR 3/4) but is also variable throughout this interval. Slightly paler colors are present in intervals that contain increased carbonate content. Diatoms, radiolarians, and foraminifers occur in only trace quantities below 16.5 mbsf (18 mcd).

A thin (3 cm) manganese oxide-rich layer near 18 m (Section 138-854A-2H-6, 102 cm; Section 138-854C-3H-3, 140 cm; between Cores 138-854B-2H and -3H) marks a hiatus of ~3.6 m.y. duration (see "Biostratigraphy" and "Paleomagnetism" sections, this chapter). Below this layer, the sediments are metalliferous clay with zeolites.

From ~22 to 32 mbsf (~24–36 mcd), the dominant lithology is dark brown to very dark brown (10YR 3/3–10YR 2/2) metalliferous clay with zeolites (probably phillipsite). These sediments are less variable, both in color and composition, than the overlying ooze and clay. The clay content is high (70%–85%), and nannofossils (5%–15%), oxides (~10%), and zeolites (~5%) comprise minor components.

The sediment between 32 and 38 mbsf (~35–42 mcd) is clayey nannofossil ooze that is paler, more variable in color (brown to light brown, 10YR 4/6–10YR 7/3), and more intensely bioturbated than the overlying sediments. The abundance of nannofossils is ~60%, but increases to nearly 80% in two light brown beds at 33 and 34.5 mbsf.

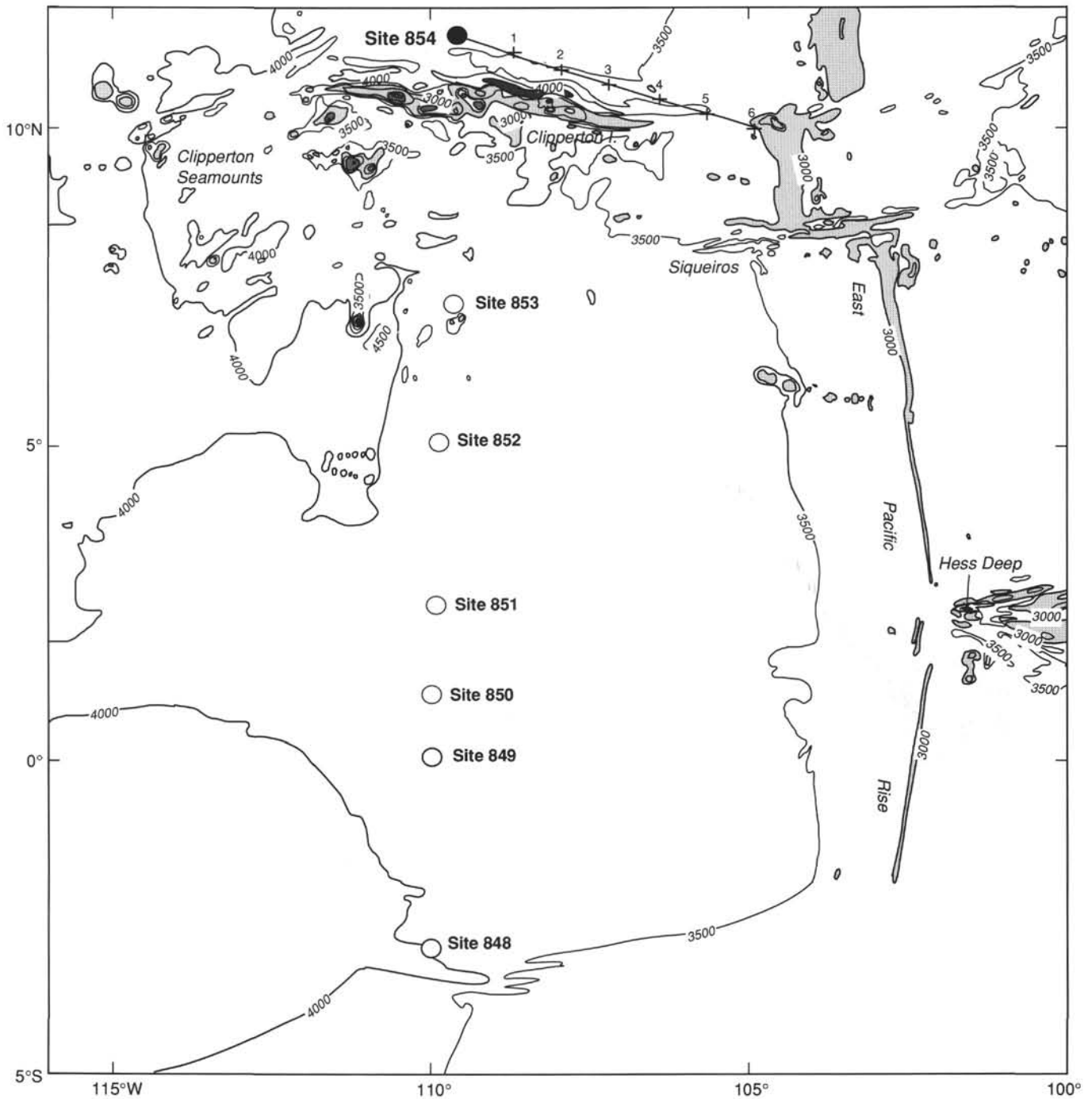


Figure 2. Generalized bathymetric map showing location of Site 854 and other Leg 138 sites drilled along the 110°W transect (from Mammerickx, 1989). Backtrack path for Site 854 (using pole of rotation of van Andel et al. [1975]) is shown in 1 m.y. increments. Bathymetry in meters.

The lowermost sediments of this site consist of homogeneous, very dark brown (10YR 3/2) to black (10YR 2/1) metalliferous clays and clayey metalliferous sediments. The sediments between 38 and 41 mbsf (42–46 mcd) are metalliferous clays with 10% to 15% Fe- and Mn-oxides. Small amounts of quartz, feldspar, and volcanic glass are also present. The basal sediments are black clayey metalliferous sediments that contain up to 80% Fe- and Mn-oxides. The color reflectance of these sediments is extremely low and ranges between 10% and 15% for all color bands (Fig. 9). The upper portion of this interval occurs in both Cores 138-854C-5H and -6H. The APC was pulled back 4 m after Core 138-854C-5H to avoid hitting the base-

ment. Apparently, the drill string moved sideways in the hole sufficiently so that this interval was re-cored in Core 138-854C-6H. No visible sign of disturbance is seen in the core.

### Color Reflectance Spectroscopy

The sedimentary sequence has relatively high reflectance in the blue, red, and near-infrared (nIR) bands at 0 to 18 mbsf (0–19.5 mcd) and at 32 to 38 mbsf (35–42 mcd) (Fig. 9). These intervals have higher carbonate content (nannofossils plus foraminifers) and lower clay content (Fig. 8) than the intervals from 18 to 32 mbsf and 38 mbsf to

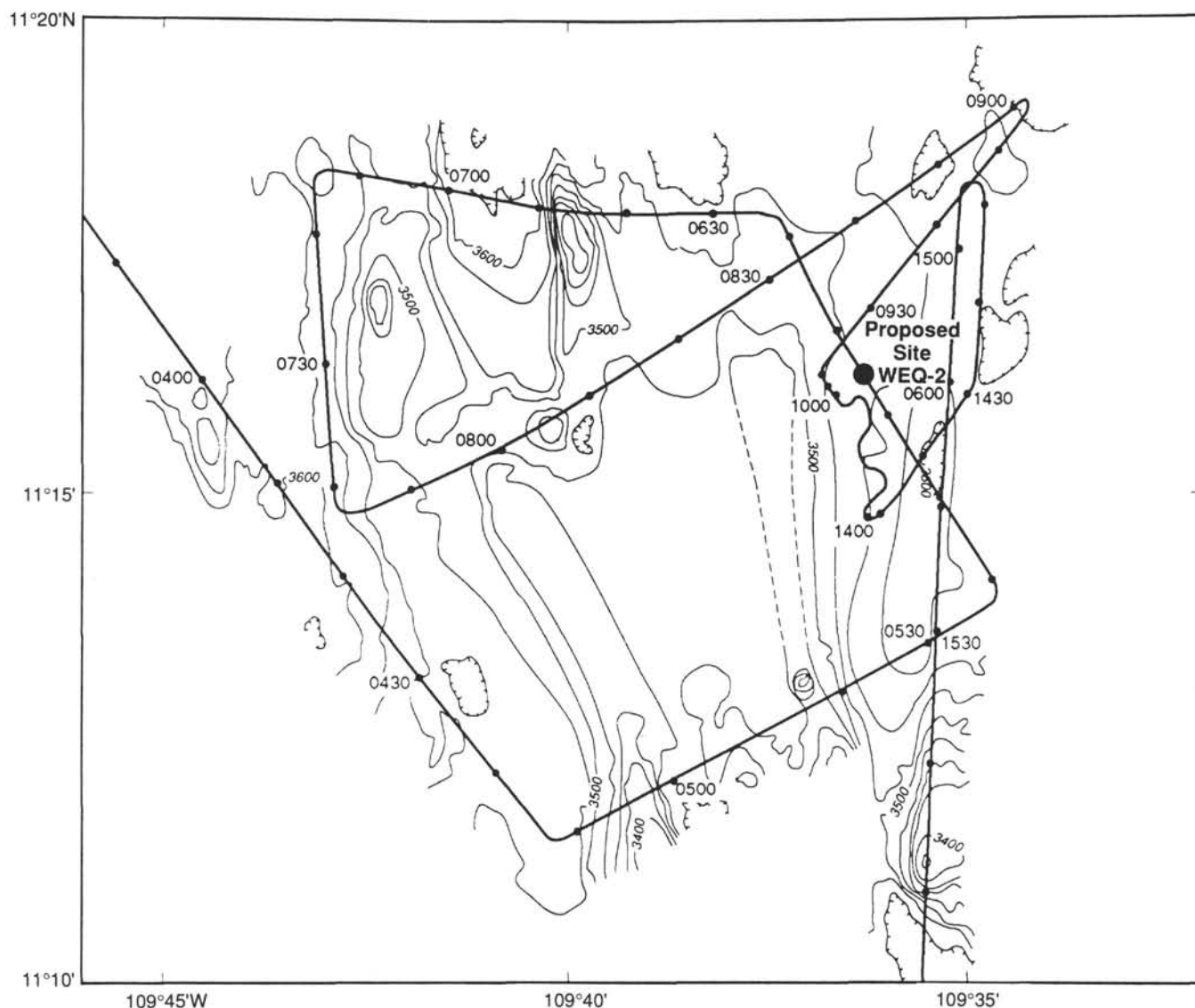


Figure 3. SeaBeam map hand-contoured from navigation-adjusted SeaBeam contour maps collected from the *Thomas Washington* during the Venture 1 cruise, September 1989. Location of proposed Site WEQ-2 is shown.

basement. The spectral patterns of two carbonate-rich lithologies, clayey nannofossil foraminifer ooze, and of clayey nannofossil ooze (Fig. 9) show that reflectance is higher across the entire range of wavelengths measured relative to metalliferous clay and clayey metalliferous sediment.

Although the first-order spectral character of the entire sedimentary sequence may be related to the relative proportion of carbonate to clay, not all bands show the same amplitude of variation from one lithologic type to the next, e.g., reflectance in the red band decreases more across the transition at 18 mbsf than in the blue or nIR bands. Across the transition at 38 mbsf from clayey nannofossil ooze to clayey metalliferous sediments, reflectance in the nIR band decreases more than in the blue or the red bands. Because variations in the reflectance of different bands are not the same across lithologic transitions, ratios can be used to characterize sediment types, e.g., the nIR/red ratio is highest for the clay-rich sediments of Site 854 (19.5–35 mcd and 42–51 mcd) (see Figs. 9 and 10). These intervals of high nIR/red are also maxima in susceptibility (Fig. 9), except for the bottom interval between 46 mcd and basement. The spectral

pattern of the clayey metalliferous sediment of this bottom interval has low reflectance across all wavelengths, while the metalliferous clay has relatively high reflectance in the nIR bands (Fig. 9). The low nIR/red values of the metalliferous sediment may be related to high ( $\leq 75\%$ ) oxide contents. Thus, while high nIR/red values do appear to characterize the clay-rich intervals, low values characterize both the oxide-rich bottom interval and the carbonate-rich intervals.

#### Relationship of Lithology to Magnetic Susceptibility

The magnetic susceptibility of Site 854 sediments increases dramatically between 16 and 20 mbsf (19–22 mcd, Fig. 10). This increase occurs over the transition from nannofossil ooze to clay with zeolites and oxides (Figs. 8 and 11). The clay fraction, inferred to be terrigenous, and the Fe- and Mn-oxide fraction of the sediment increase over this interval. The low susceptibility of both carbonate-rich intervals discussed above suggests that the overall pattern of susceptibility may reflect the dilution of magnetic minerals with calcareous sediment.

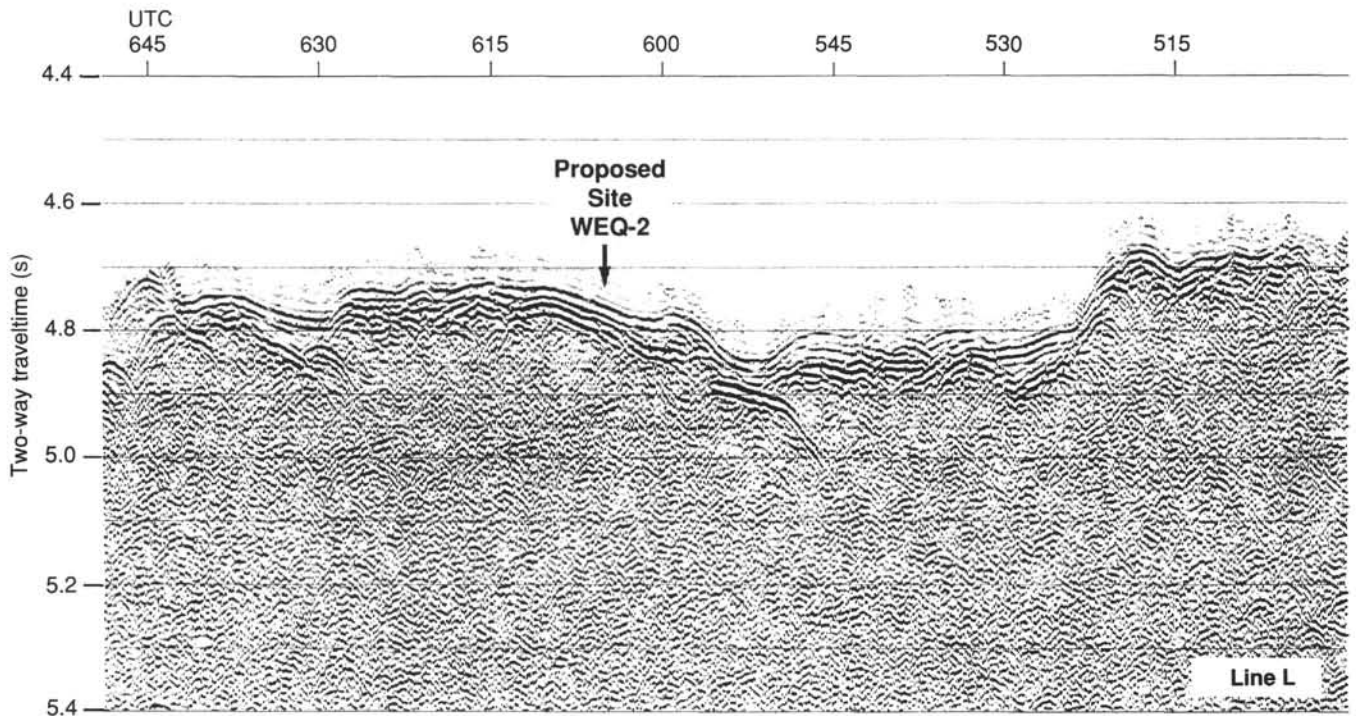


Figure 4. Digital seismic line collected with an 80-in.<sup>3</sup> water gun during the *Thomas Washington* cruise, Venture 1. Location of proposed Site WEQ-2 is shown.

### Trace Fossils

Bioturbation is strong within the upper 22 m of sediment. Solid burrows and rind burrows are abundant with ovoid *Planolites* also common. *Zoophycos* are common between 5 and 16 mbsf. *Skolithos* also are present, but less common within this interval. Slight bioturbation is apparent between 22 and 32 mbsf in the dark brown oxide-rich clay. The intensity of bioturbation increases between 32 and 38 mbsf and solid burrows and *Planolites* are common. A few *Chondrites* are also present in this interval. Bioturbation appears slight in the metalliferous sediment below 38 mbsf.

### BIOSTRATIGRAPHY

Sediments recovered from Site 854 represent a stratigraphic sequence from the Quaternary through most of the upper Miocene. One stratigraphic break was placed within Section 138-854A-2H-6 and between Cores 138-854B-2H and -3H. This hiatus extends from CN12 to CN9b (NN18/16–NN11) and represents a maximum duration of 3.6 m.y.

Microfossils vary in abundance throughout the stratigraphic sequence recovered. Calcareous nannofossils, foraminifers, radiolarians, and diatoms occur in the Quaternary and upper Pliocene interval. With the exception of the foraminifers, which exhibit poor preservation, microfossils generally exhibit moderate to good preservation. Below the unconformity, foraminifers and siliceous microfossils are generally absent. Calcareous nannofossils do occur in this lower stratigraphic sequence, but their occurrence is inconsistent and their preservation is generally poor.

The lowermost sediment dated using microfossils is from Section 138-854C-6H-1, which has an age younger than 7.5 Ma (base of CN9a, NN11) (Fig. 12). The sequence below this sample is barren of microfossils. The paleomagnetic polarity sequence, which extends throughout the cored sequence, suggests that the base of the sequence may be equivalent to the upper portion of Chron C5.

Epoch boundaries identified at Site 854 are as follows:

Boundary	Hole	Depth (mbsf)	Depth (mcd)	Event
Pleistocene/Pliocene	854B	10.30	(10.60)	Olduvai (t)
	854C	9.82	(10.62)	Olduvai (t)
late/early Pliocene	854C	17.08	(19.08)	Gauss/Gilbert

(t) = termination.

### Calcareous Nannofossils

Calcareous nannofossil assemblages from the Pleistocene, upper Pliocene, and upper Miocene were observed in the sediments recovered from Site 854 (Table 2). Throughout this sequence, intervals containing calcareous nannofossils that exhibit slight or extreme dissolution alternate with intervals that are barren of nannofossils.

Calcareous nannofossils are moderately well preserved in the Pleistocene sediments (Sections 138-854B-1H-1 through -2H-1). Within this interval, some placoliths are partially dissolved, and the assemblage is characterized by abundant *Pseudoemiliania lacunosa* and *Gephyrocapsa oceanica* s.l. The first occurrence of *G. oceanica* s.l. approximates the Pleistocene/Pliocene boundary (top of Olduvai) and is recorded between Samples 138-854B-2H-1, 65 cm, and -2H-1, 140 cm. The interval from Sections 138-854B-2H-2 through -2H-CC is placed in the upper Pliocene Zone CN12 (NN18–16). The nannofossil assemblage in this interval is rich and moderately well preserved.

At the top of Core 138-854B-3H (Sections 138-854B-3H-1 through -3H-4), a dissolved nannofossil assemblage of upper Miocene Zone CN9b (NN11) is observed and is characterized almost entirely by discoasterids, with rare *Amaurolithus* spp. and *Triquetrorhabdulus rugosus* specimens. The stratigraphic break between Cores 138-854B-2H and -3H represents a hiatus with a maximum duration of

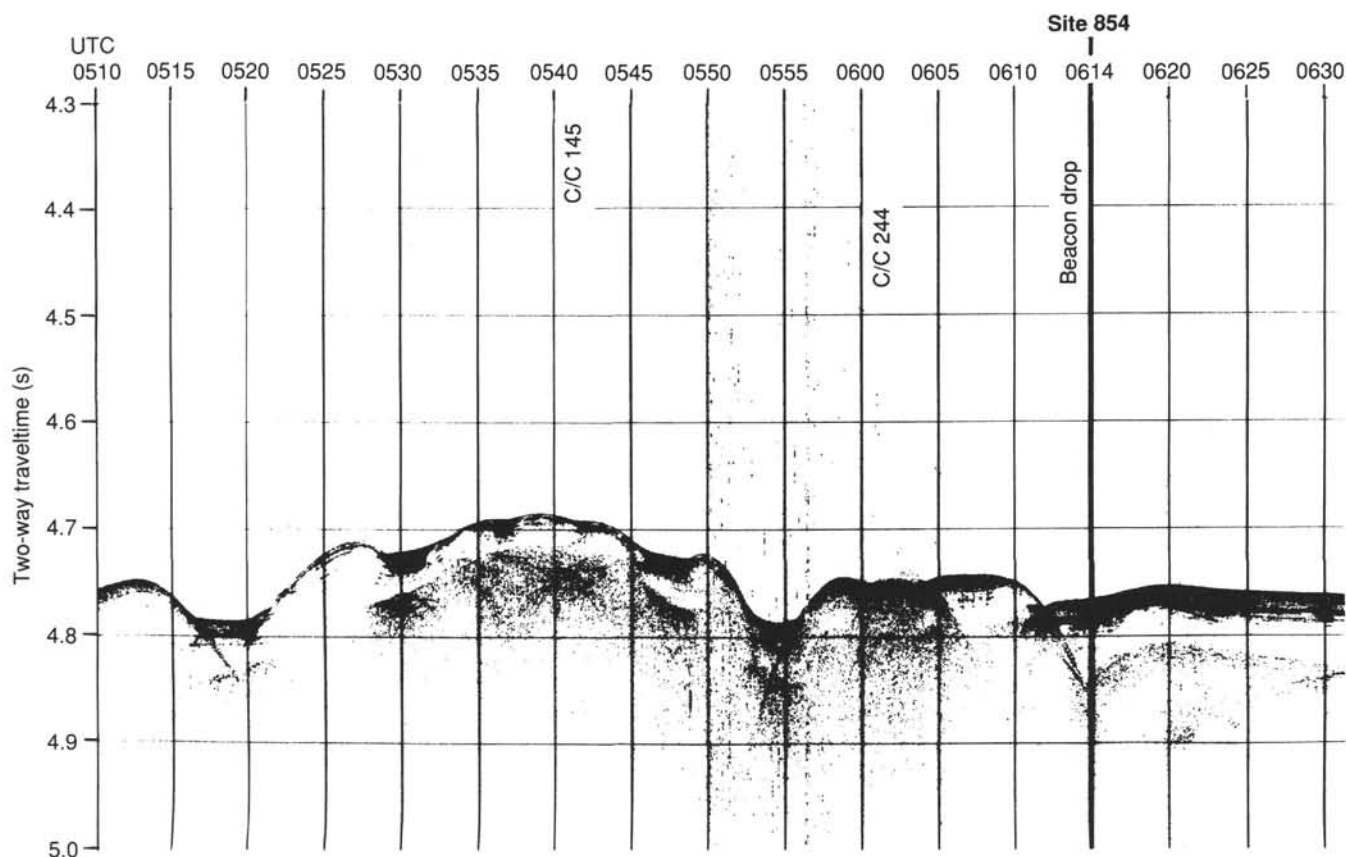


Figure 5. 3.5 kHz profile collected from *JOIDES Resolution* during site survey showing location of Site 854.

~3.6 m.y. This hiatus is also recorded in Hole 854A within Section 138-854A-2H-6.

Calcareous nannofossils are absent in samples from Sections 138-854B-3H-5 through -3H-CC. They reappear at the top of Core 138-854B-4H, as a dissolved assemblage characterized by rare discoasterids typical of the upper Miocene Zone CN9 (NN11). Although samples examined from Cores 138-854B-5H, -854C-5H and -6H are generally barren of calcareous nannofossils, occasionally poorly preserved assemblages were observed. The nannofossils observed in

Sections 138-854B-5H-1 and -854C-6H-1, indicate an age younger than 7.5 Ma for this lower interval of Site 854 (Cores 138-854B-5H and -854C-6H). The lowermost part of the sequence (Sections 138-854C-6H-2 through -6H-CC) is barren of nannofossils.

### Planktonic foraminifers

Planktonic foraminifers are common in the uppermost interval (0–2 cm) of Core 138-854B-1H and few in Sample 138-854A-1H-

**Table 1. Summary of coring operations at Site 854.**

Core no.	Date (June 1991)	Time (UTC)	Depth (mbsf)	Length cored (m)	Length recovered (m)	Recovery (%)
138-854A-1H	28	1245	0.0–9.9	9.9	9.96	100.0
2H	28	1435	9.9–19.4	9.5	9.97	105.0
3X	28	1430	19.4–28.7	9.3	0.96	10.3
Coring totals				28.7	20.89	72.8
138-854B-1H	28	1650	0.0–8.4	8.4	8.38	99.7
2H	28	1740	8.4–17.9	9.5	9.64	101.0
3H	28	1835	17.9–27.4	9.5	10.05	105.8
4H	28	1925	27.4–36.9	9.5	9.95	105.0
5H	28	2015	36.9–45.4	8.5	9.99	117.0
Coring totals				45.4	48.01	105.7
138-854C-1H	28	2145	0.0–3.6	3.6	3.60	100.0
2H	28	0002	3.6–13.1	9.5	10.12	106.5
3H	28	2325	13.1–22.6	9.5	10.01	105.3
4H	29	0020	22.6–32.1	9.5	10.06	105.9
5H	29	0110	32.1–41.6	9.5	10.13	106.6
6H	29	0255	41.6–46.0	4.4	10.11	229.8
Coring totals				46.0	54.03	117.4

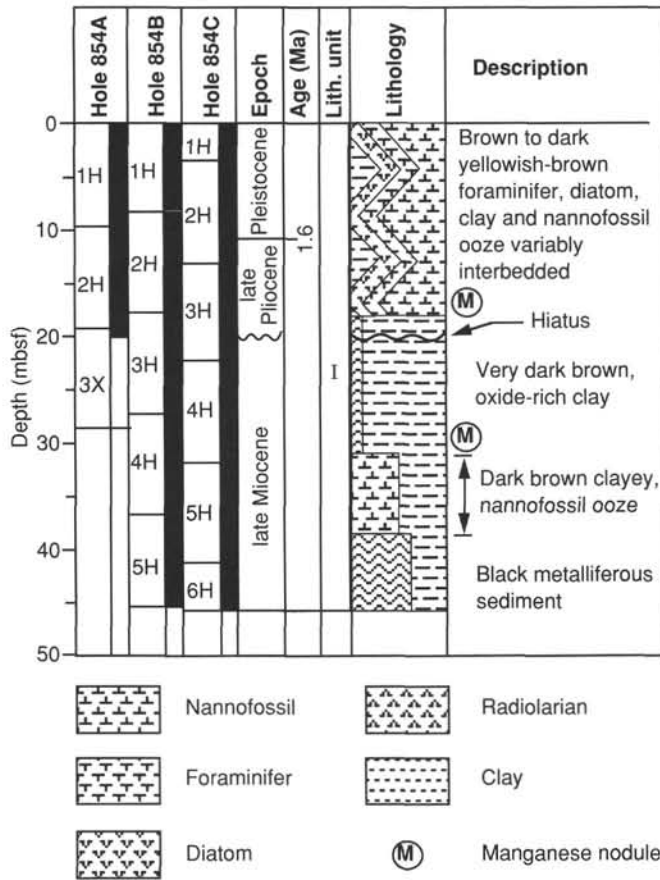


Figure 6. Lithostratigraphic summary of Site 854.

CC; in both samples, preservation is poor. The foraminiferal assemblages exhibit a high degree of fragmentation and consist mainly of the robust species *Globorotalia tumida* and numerous keel fragments of this species. No planktonic foraminifers were observed in the remainder of the sedimentary sequence.

The main components of the coarse fraction residues include (1) benthic foraminifers, which are few to abundant in Samples 138-854A-1H-CC through -3X-CC and -854B-4H-CC; (2) radiolarians, which are few to common in Core 138-854A-1H; (3) sponge spicules, which are abundant in Sample 138-854A-1H-CC; (4) volcanic glass, which is abundant in the upper portion of Core 138-854A-3X and common in Sample 138-854B-5H-CC; and (5) manganese micronodules, which are abundant in Sample 138-854A-3X-CC.

**Radiolarians**

Radiolarians sampled at Site 854 are from the Quaternary and upper Pliocene. Below the top of Core 138-854B-3H, all samples examined are barren of siliceous microfossils. Trace fragments of tests were found in a few of the deeper samples; however, these were never adequate for an evaluation of the age of the sediment or the character of the assemblage. Within the upper two cores of Hole 854B (upper Pliocene through Pleistocene), preservation of the radiolarians is moderate. Most of the major radiolarian datums and all of the radiolarian zones down through the *Stichocorys peregrina* Zone can be identified (Table 3). A broken specimen of *Phormostichoartus fistula* occurs in Sample 138-854B-2H-7, 36 cm, suggesting that the base of the *S. peregrina* Zone may lie at or slightly above this sample.

Although the age of the section containing preserved siliceous microfossils is only slightly older at this site than it is at Site 853 to the south, the degree of preservation of the fauna is somewhat better and the amount of reworked older microfossils is smaller. Reworking of upper Miocene radiolarians (from the *Diartus petterssoni* Zone) was found in only one sample (138-854B-1H-3, 110 cm; from the *Amphirhopalum ypsilon* Zone). As at Site 853, we were surprised to

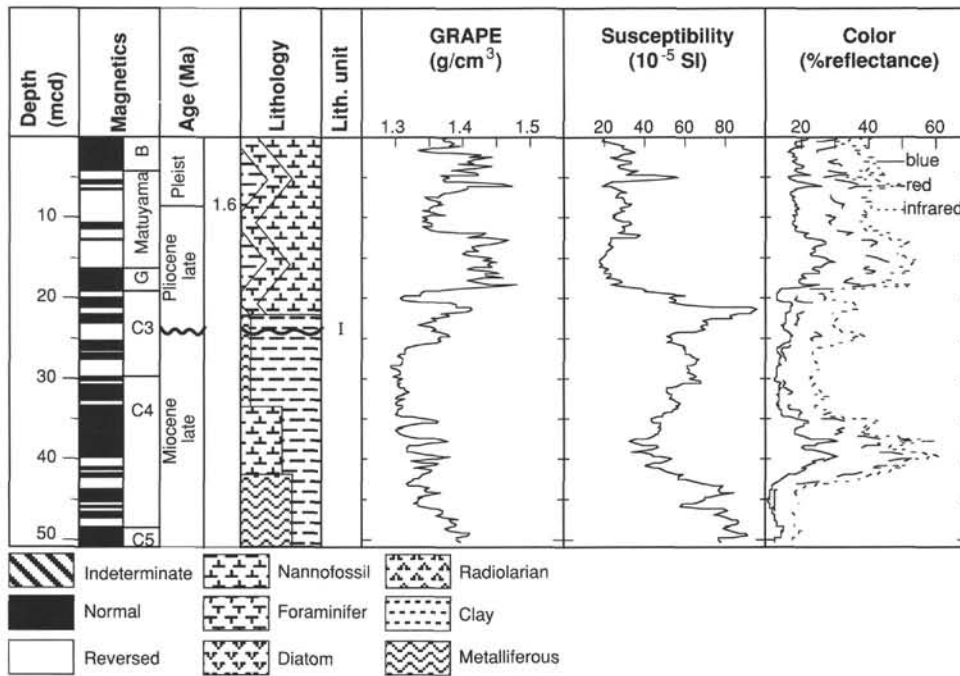


Figure 7. Composition summary of magnetics, age, graphic lithology, GRAPE density, magnetic susceptibility, and percentage of color reflectance for Site 854. The composite data consist of sections spliced together from the multiple holes drilled at the site. Data are shown plotted vs. meters composite depth (mcd), the new depth scale used when constructing composite sections. GRAPE, susceptibility, and color data have been smoothed using a 20-point Gaussian filter.



**Table 2. Sample and depth constraints of calcareous nannofossil events for Site 854.**

Event	Hole 854B interval (cm)	Depth (mbsf)	Depth (mcd)
T <i>Pseudoemiliania lacunosa</i>	1H-2, 80–1H-3, 25	2.39–3.25	2.30–3.25
B <i>Gephyrocapsa</i> sp. 3	1H-4, 65–1H-4, 130	5.15–5.80	5.15–5.80
T <i>Calcidiscus macintyre</i>	2H-1, 65–2H-1, 140	9.05–9.80	9.35–10.10
B <i>Gephyrocapsa oceanica</i> s.l.	2H-1, 65–2H-1, 140	9.04–9.80	9.35–10.10
T <i>Discoaster pentaradiatus</i>	2H-5, 25–2H-5, 65	14.65–15.05	14.95–15.35
T <i>Discoaster surculus</i>	2H-5, 130–2H-6, 25	15.70–16.15	16.00–16.45

find comparatively well-preserved Miocene forms in a more poorly preserved, younger assemblage when the upper Miocene section at this site does not appear to contain any siliceous microfossils. This suggests that upper Miocene siliceous microfossils were deposited in this region. They may have been removed from the thicker sections by post-depositional dissolution, but have been preserved in nearby outcrops of upper Miocene sediments.

### Diatoms

Diatoms are present only in the uppermost portion (Sections 138-854B-1H-1 through -2H-5) of the stratigraphic sequence recovered from Site 854. Rare to few diatoms exhibiting moderate preservation are observed in this interval. The diatom assemblage present is typified by *Azpeitia nodulifer* and *Hemidiscus cuneiformis*. Age-diagnostic species are rare throughout this interval.

Sample 138-854C-1H-CC was assigned to the *Pseudoemiliania doliolus* Zone, based on the occurrence of *P. doliolus* without *Nitzschia*

**Table 3. Sample and depth constraints of radiolarian events for Site 854.**

Event	Hole 854B interval	Depth (mbsf)	Depth (mcd)
T <i>Stylatractus univertus</i>	1H-2–1H-3	2.60–3.40	2.60–3.40
B <i>Collasphaera tuberosa</i>	1H-2–1H-3	2.60–3.40	2.60–3.40
T <i>Lamprocyrtis neoheteroporos</i>	1H-3–1H-4	4.10–5.60	4.10–5.60
T <i>Anthocyrtidium angulare</i>	1H-5–1H-5	6.40–7.10	6.40–7.10
T <i>Theocorythium vetulum</i>	1H-5–1H-5	6.40–7.10	6.40–7.10
B <i>Lamprocyrtis nigriinae</i>	1H-5–1H-6	7.10–7.90	7.10–7.90
B <i>Theocorythium trachelium</i>	1H-CC–2H-1	8.38–8.80	8.38–9.10
B <i>Pterocorys minyothorax</i>	2H-1–2H-2	9.50–10.30	9.80–10.60
B <i>Anthocyrtidium angulare</i>	2H-2–2H-2	10.30–11.0	10.60–11.30
T <i>Pterocanium prismatium</i>	2H-2–2H-2	10.30–11.0	10.60–11.30
T <i>Lamprocyrtis heteroporos</i>	2H-1–2H-2	9.50–10.30	9.80–10.60
T <i>Anthocyrtidium genghisi</i>	2H-4–2H-5	14.00–14.80	14.30–15.10
B <i>Theocalyptra davisiana</i>	2H-5–2H-5	14.80–15.50	15.10–15.80
T <i>Stichocorys peregrina</i>	2H-5–2H-6	15.50–16.30	15.80–16.60
T <i>Phormostichoartus fistula</i>	2H-6–2H-7	17.00–17.76	17.30–18.06

*reinholdii*. Samples 138-854A-1H-CC and -854B-1H-CC were assigned to Subzone B of the *Nitzschia reinholdii* Zone. This age assignment was based on the occurrence of *Nitzschia fossilis*, *N. reinholdii*, and *P. doliolus* in these samples without *Rhizosolenia praebergonii*. The occurrence of the silicoflagellate *Mesocena quadrangula* in Sample 138-854B-1H-CC supports this zonal assignment. With the exception of Sample 138-854B-2H-5, 70 cm, samples examined from Core 138-854B-2H either contain nonage-diagnostic species or are barren of diatoms. The occurrence of *Thalassiosira convexa* var. *convexa* in Sample 138-854B-2H-5, 70 cm, suggests that this sample is older than 2.1 Ma. Samples examined below Core 138-854B-2H are barren of diatoms.

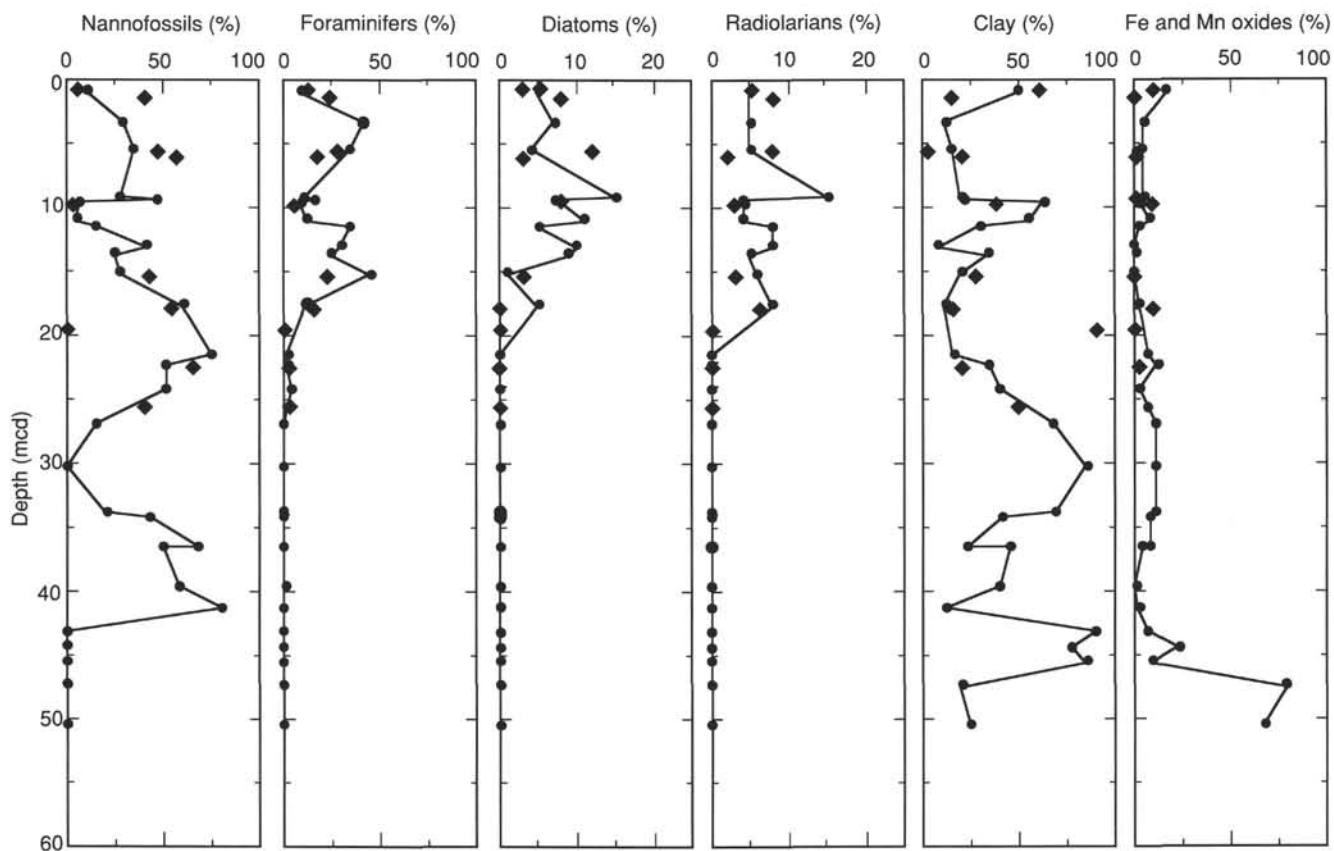


Figure 8. Summary of major (line with symbols) and minor (symbols only) component smear slide data from Site 854.

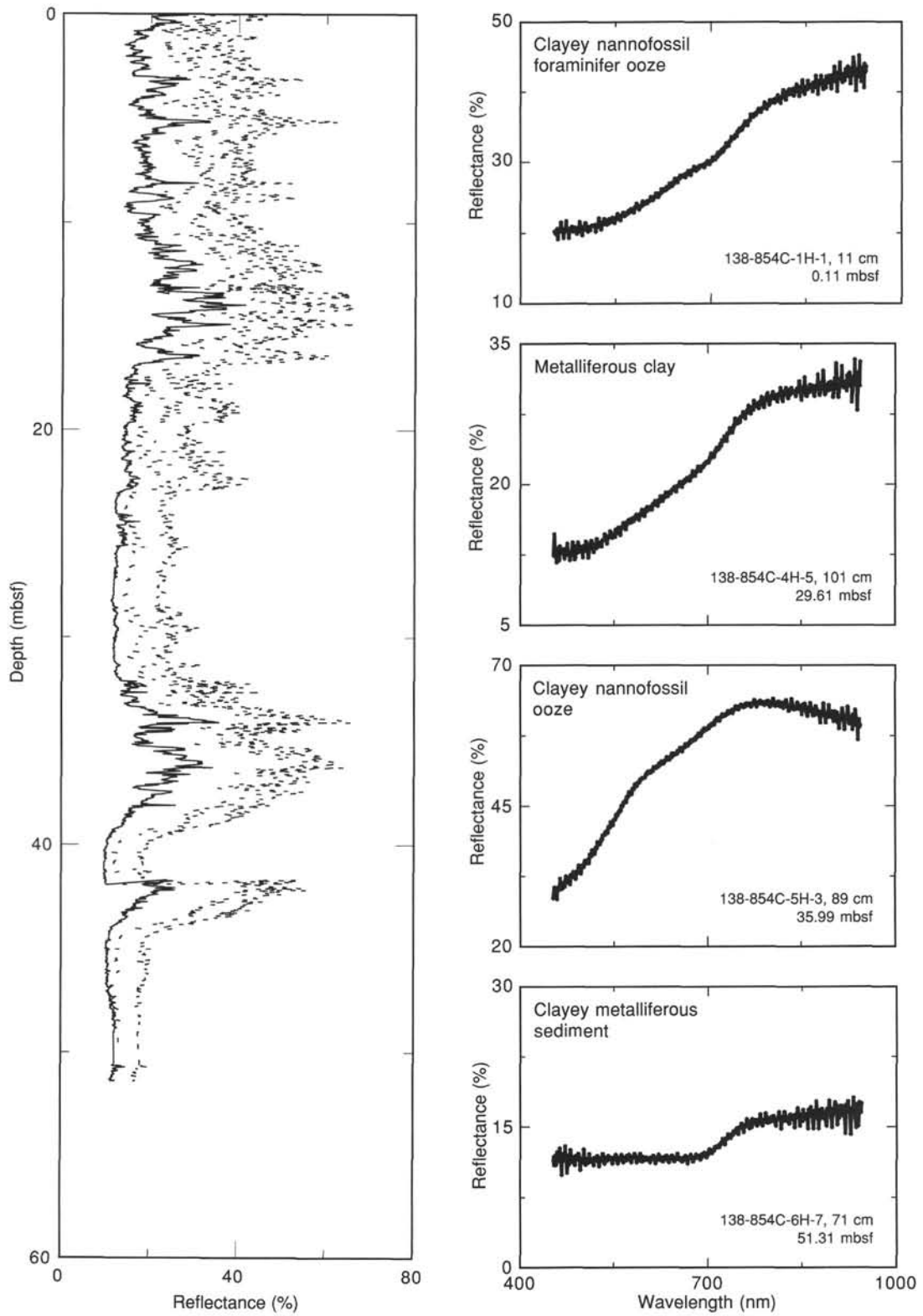


Figure 9. Downhole summary of color reflectance data for Hole 854B (left), blue (solid line); red (dashed line); near-infrared (dotted line). Examples of reflectance spectra for specific lithologies within the core are shown at right.

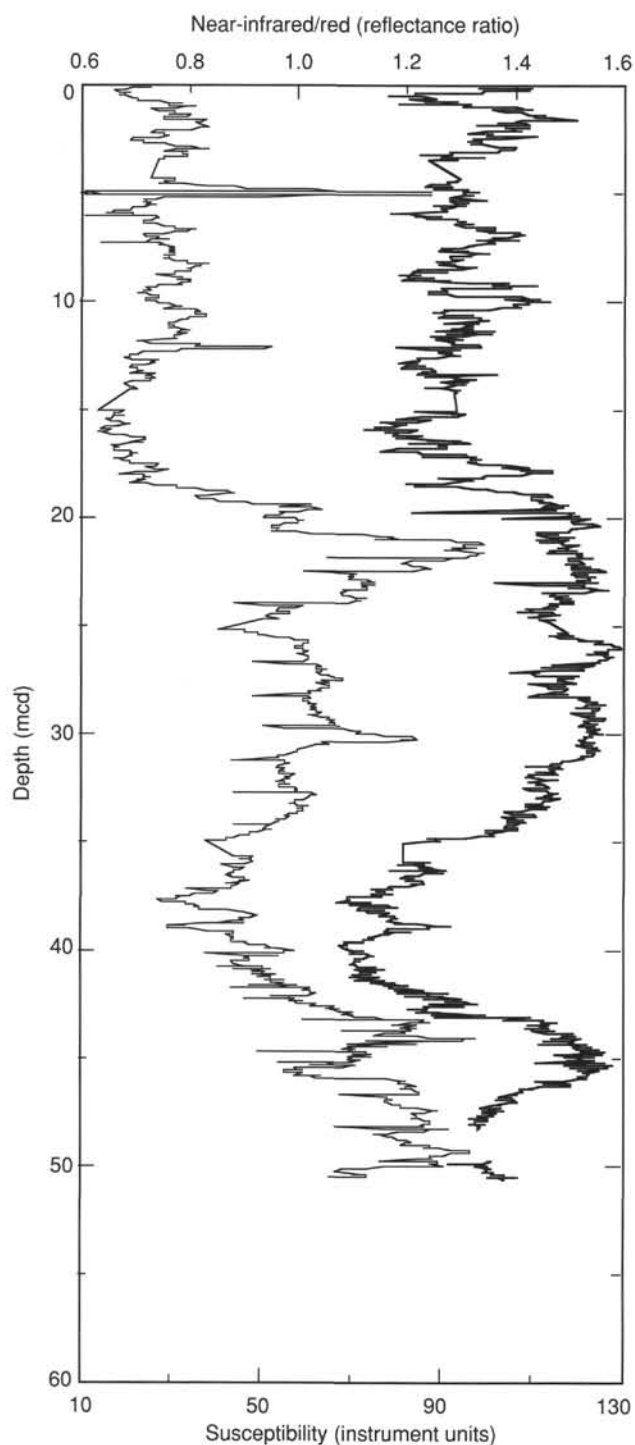


Figure 10. nIR/red color reflectance ratios (thin line) and susceptibility (thick line) for Hole 854C.

## PALEOMAGNETISM

### Laboratory Procedures

Paleomagnetic measurements at Site 854 followed the methods discussed in the "Explanatory Notes" chapter (this volume). The relatively thin sedimentary section at this site was entirely APC-cored, except for a short XCB core from Hole 854A. We measured the natural and the 15-mT demagnetized remanence of all the recovered

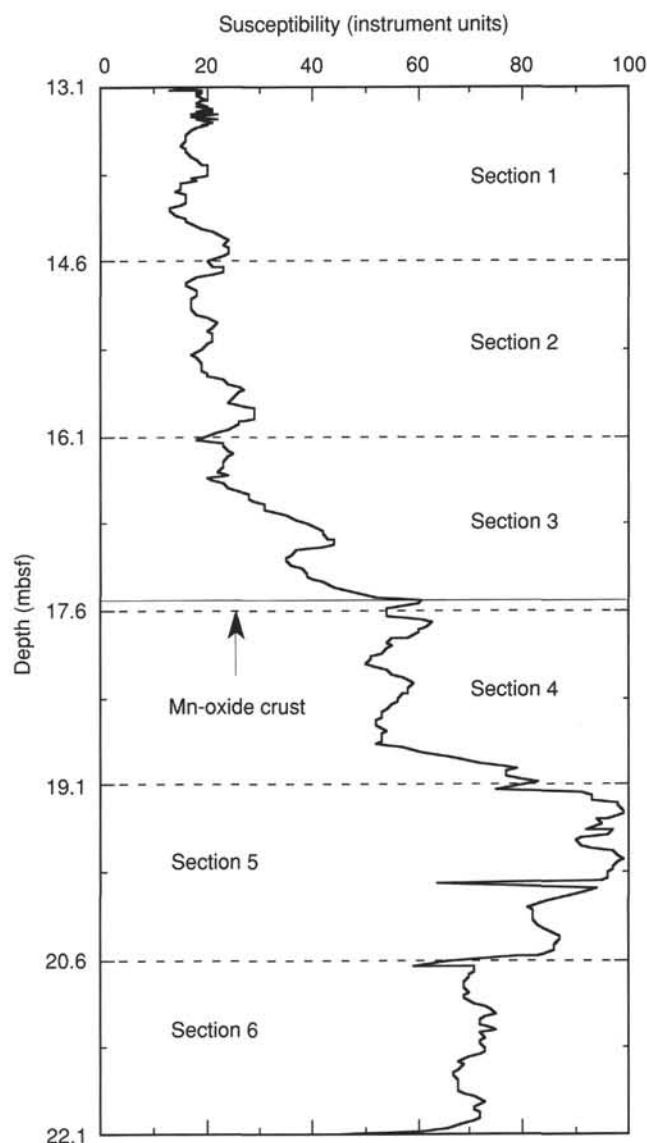


Figure 11. Susceptibility data across the transition from nannofossil ooze to clay with zeolites and oxides in Core 138-854C-3H.

sediments. Remanence at Site 854 was relatively stable, and 15-mT alternating field (AF) demagnetization was usually sufficient to remove the pervasive drilling overprint and to reveal the magnetic polarity zonation. We have correlated this zonation with the magnetic polarity time scale (MPTS), using the constraints provided by the nannofossil biostratigraphy. As at other Leg 138 sites, our magnetostratigraphic interpretations are based entirely on this 15-mT AF demagnetized remanence.

Following standard Leg 138 procedures, the susceptibility of unsplit core sections was routinely measured using the multisensor track (MST). Cores 138-854A-1H to -854B-3H-4 were measured at 5-cm intervals on the high sensitivity scale (0.1), and Cores 138-854B-3H-5 to the bottom of Hole 854C were measured at 3-cm intervals on the lower sensitivity setting (1.0).

## Results and Discussion

The stability of the characteristic remanence is illustrated by the 180° declination changes at reversal boundaries, accompanied by the appropriate sense of the inclination changes (Figs. 13, 14, and 15).

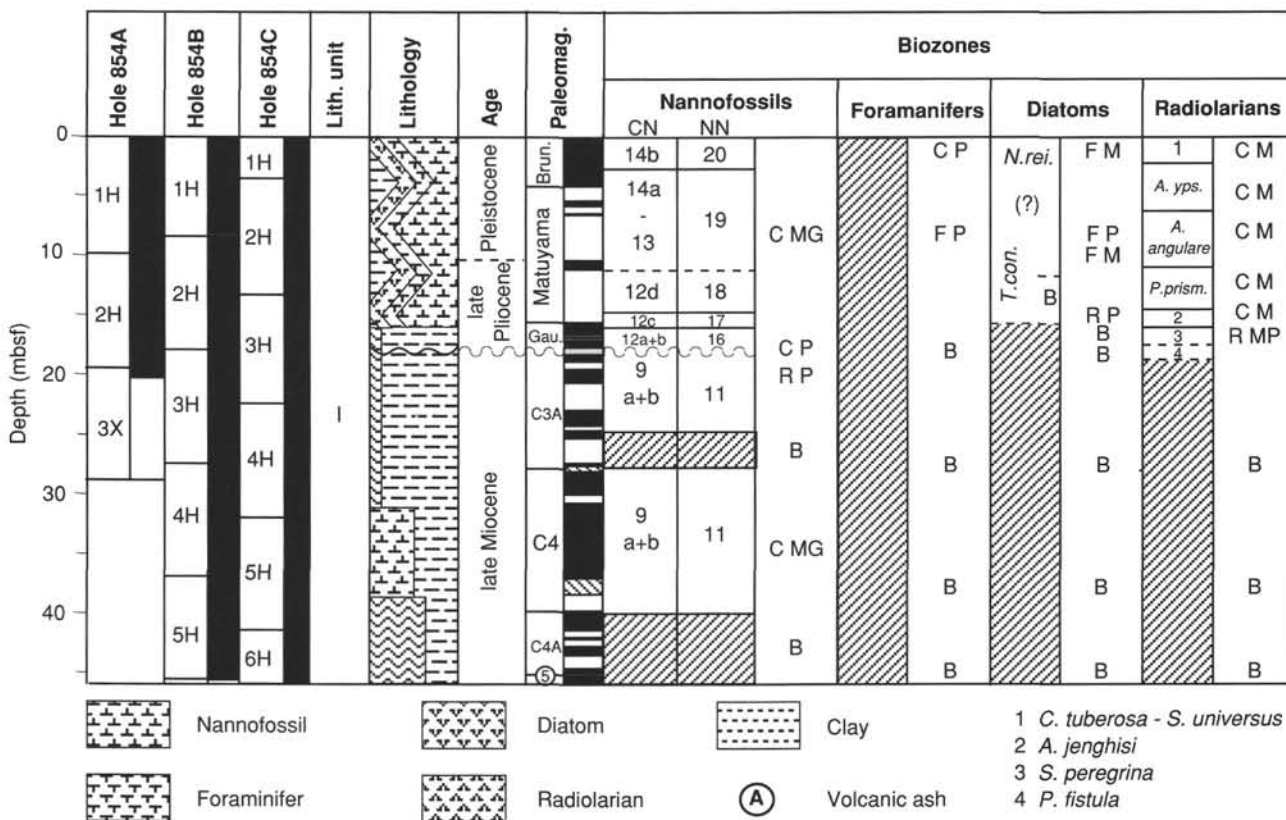


Figure 12. Stratigraphic summary for Site 854. Depth is in meters below seafloor (mbsf). Microfossil abundances recorded as A = abundant; C = common; F = few; R = rare; B = barren. Microfossil preservation recorded as G = good; M = moderate; P = poor. An "r" indicates the presence of older reworked microfossils. This figure is a general overview of the stratigraphic results at Site 854. Placement of specific stratigraphic boundaries may differ slightly between holes. Data presented here are based on results from Hole 854B.

Note that inclinations are slightly skewed to negative values, indicating that a residual from the drilling overprint remains. Because of the relatively high stability of the characteristic remanence, no discrete samples were measured onboard the ship at Site 854.

No multishot orientations were obtained for Site 854. However, the completely recovered composite section from the three holes, together with the inclination and declination patterns, enabled us to

Table 4. Secondary core orientations for Site 854.

Hole	Angle (degrees)
<sup>a</sup> 854A-1H	320
<sup>a</sup> 854A-2H	70
<sup>a</sup> 854B-1H	290
<sup>a</sup> 854B-2H	170
<sup>a</sup> 854B-3H	200
<sup>a</sup> 854B-4H	280
<sup>a</sup> 854B-5H	270
<sup>a</sup> 854C-1H	105
<sup>a</sup> 854C-2H	150
<sup>a</sup> 854C-3H	5
<sup>a</sup> 854C-4H	180
<sup>a</sup> 854C-5H	150
<sup>a</sup> 854C-6H	70

<sup>a</sup> Secondary orientation (SOR) angle is the value used to adjust average measured declination to 0° or 180° for normal or reversed chronozones, respectively, when no multishot orientation was available.

make a reasonably unambiguous selection of polarity sense in each core. Secondary orientations of the cores are given in Table 4. In Core 138-854B-5H, for example, the inclination fluctuations did not permit ready polarity assignments (Fig. 14); however, the overlapping segment in Hole 854C, independently determined with GRAPE and susceptibility data, provided unambiguous polarity determinations for the base of the section.

Susceptibilities at Site 854 are generally higher than those at previous Leg 138 sites, which is consistent with the higher clay content and greater proportion of terrigenous sediments at this location. At 19.5 mcd, a Mn-rich layer was recovered in Holes 854A and 854C (18.5 mbsf). At this depth, an abrupt increase occurs in susceptibility from values of 10 to 20 × 10<sup>-5</sup> SI to values between 30 and 50 × 10<sup>-5</sup> SI (Fig. 16). Nannofossil stratigraphy (see "Biostratigraphy" section, this chapter) indicates a hiatus at this Mn-rich layer, with middle Pliocene microfossils just above and upper Miocene microfossils just below this boundary.

The intensity of the natural remanent magnetization (NRM), which largely reflects the drilling overprint, is similar to the susceptibility profile (Fig. 16). However, Site 854 is the only Leg 138 site where the profile of the characteristic magnetization intensity does not substantially mimic the susceptibility pattern. The intensity of the "cleaned" remanence is greatest in the upper few (~4 m), fluctuating between 5 and 10 mA/m; it then decreases down the section. No abrupt change in intensity at the Mn-rich layer was seen; however, the average intensity below the Mn-rich layer was significantly lower and varied between 1 and 5 mA/m, with no discernable trend down-hole. The profile of the magnetization intensity is consistent with dilution in the deeper part of the section, as indicated by the higher

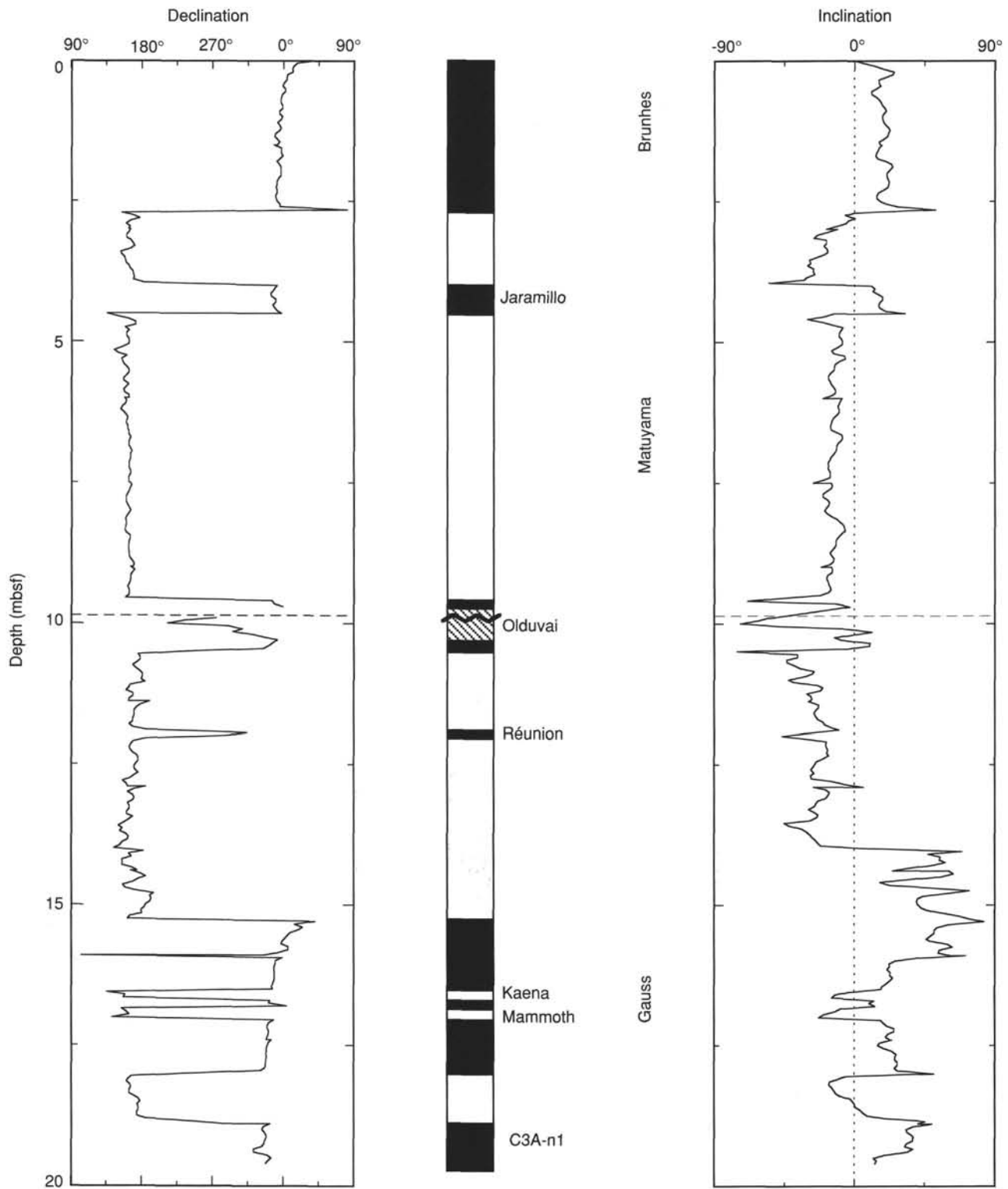


Figure 13. Declination and inclination profiles from the pass-through magnetometer, demagnetized at 15 mT, and identification of polarity chronozones in Hole 854A. Black = normal, white = reverse, hatched = no data or no interpretation. Dashed lines indicate core boundaries. Declinations have been rotated as described in Table 4.

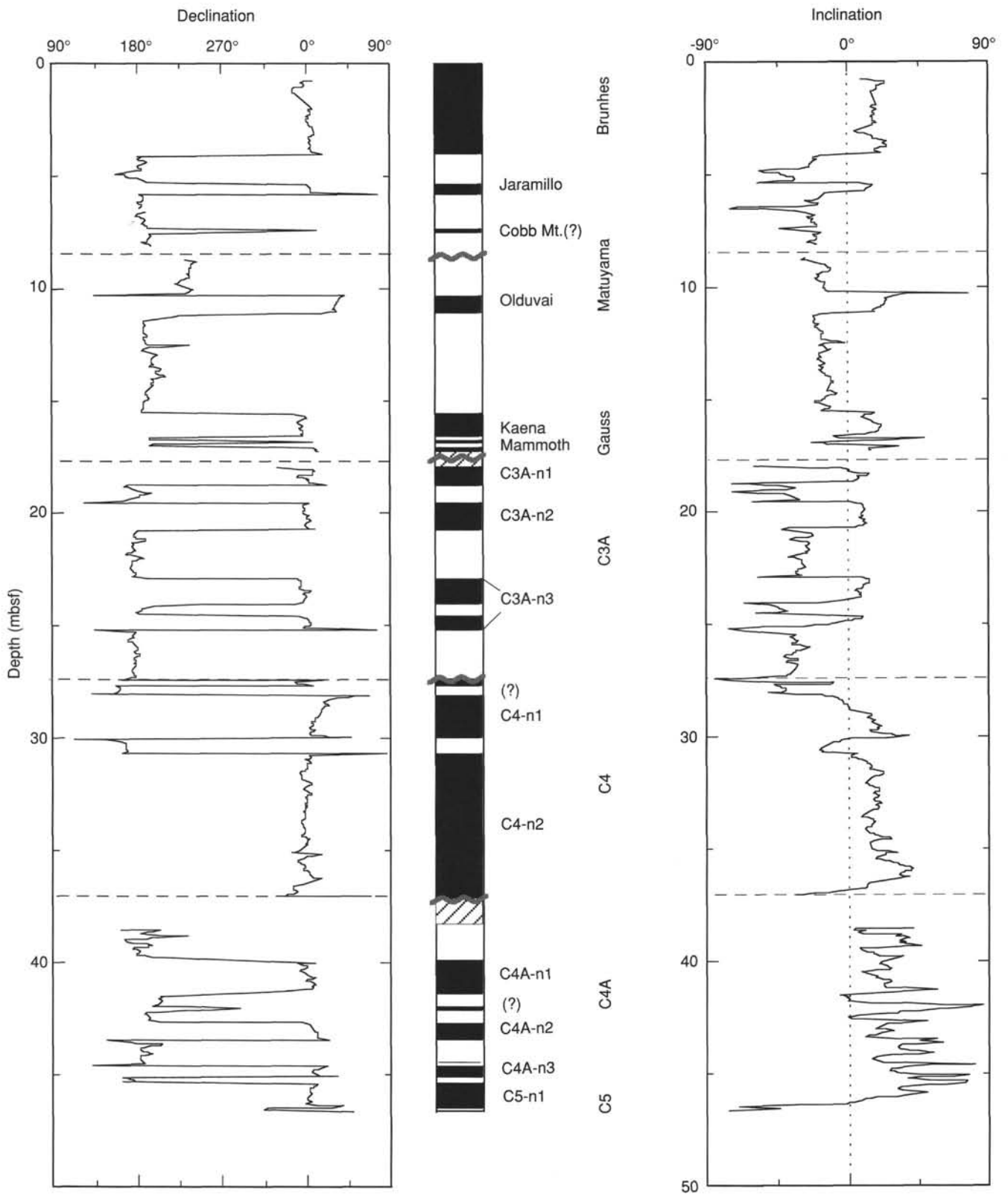


Figure 14. Declination and inclination profiles from the pass-through magnetometer, demagnetized at 15 mT, and identification of polarity chronozones in Hole 854B. Black = normal, white = reverse, hatched = no data or no interpretation. Dashed lines = core boundaries. Declinations have been rotated as described in Table 4.

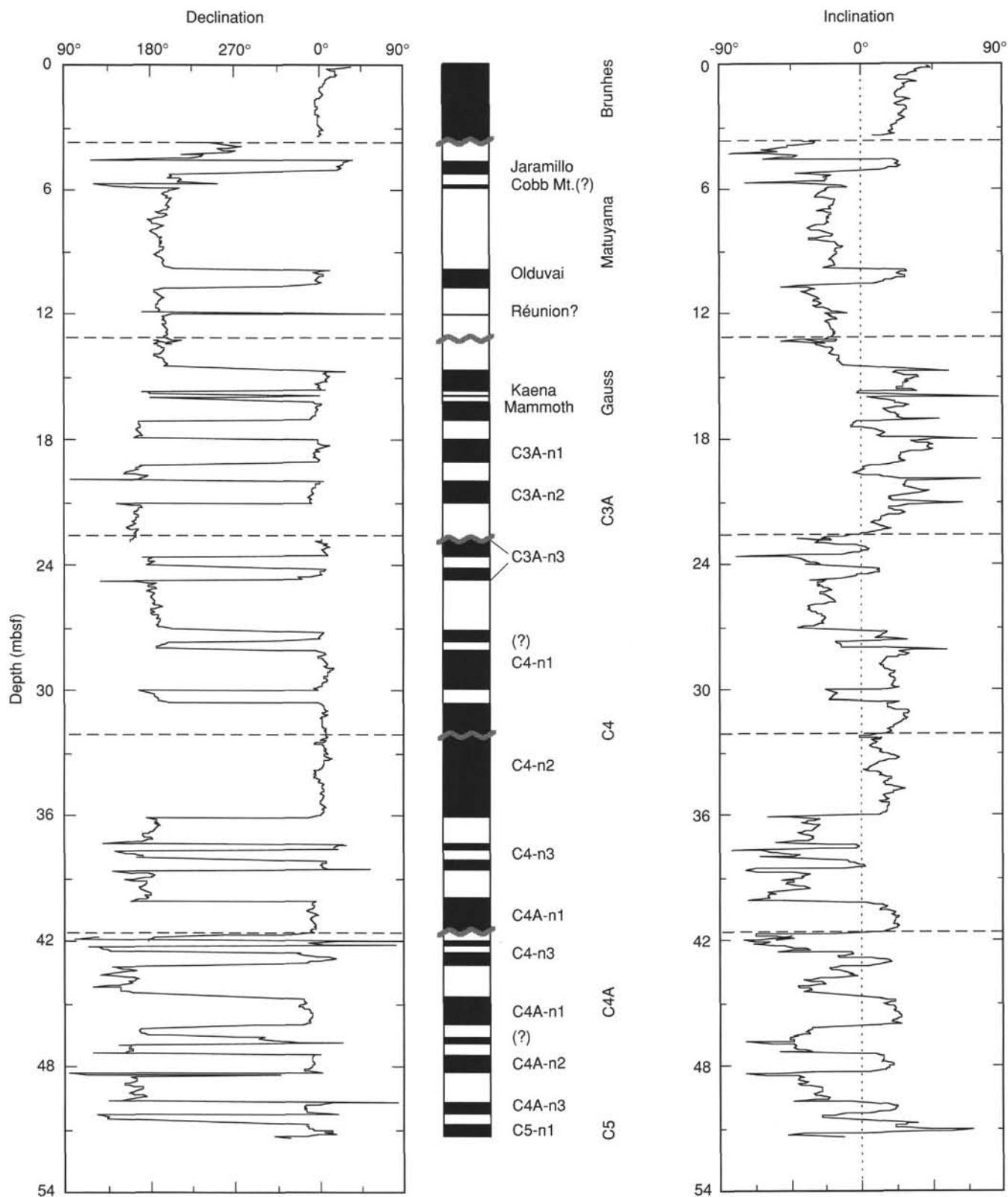


Figure 15. Declination and inclination profiles from the pass-through magnetometer, demagnetized at 15 mT, and identification of polarity chronozones in Hole 854C. Black = normal, white = reverse, hatched = no data or no interpretation. Dashed lines = core boundaries. Declinations have been rotated as described in Table 4.

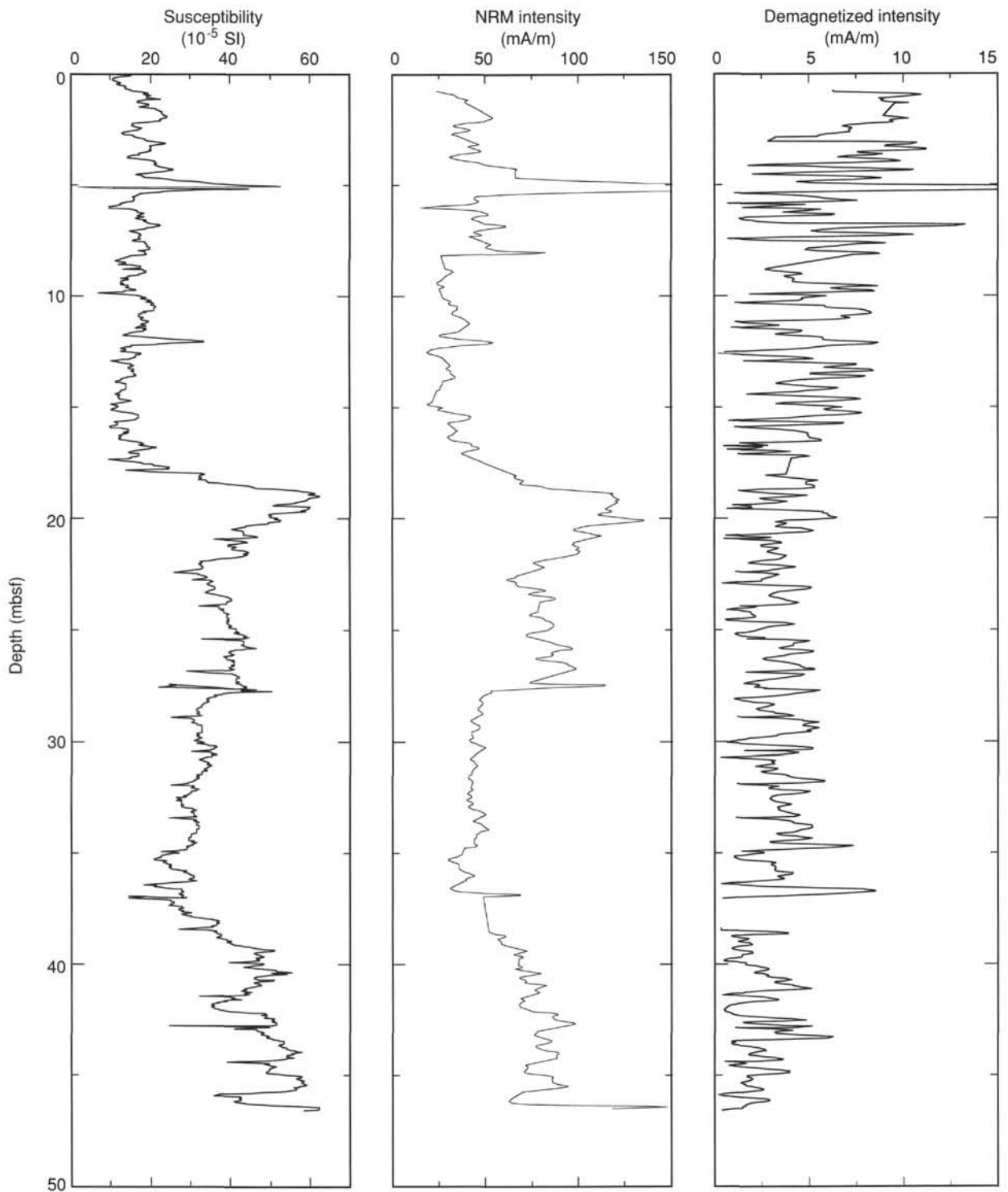


Figure 16. Downhole trends of the susceptibility, NRM, and 15 mT demagnetized remanence intensity in Hole 854B. The similar trends of the susceptibility and NRM intensity (which is primarily a drilling-induced remanent magnetization) reflect the total amount of magnetizable material in the sediment. The different downhole trend of the stable remanence indicates that it resides in a different particle distribution than that which gives rise to susceptibility.



carbonate contents and higher sedimentation rates below the Mn-rich layer. Clearly, the intensity of stable magnetization and susceptibility responds differently at Site 854.

Above the hiatus, the magnetic polarity zones can be readily correlated with the MPTS in a manner that is consistent with the biostratigraphy. The composite record includes every chronozone to the base of the Gauss at 3.4 Ma, with an average sedimentation rate of ~5.6 mcd/m.y. Despite this relatively low sedimentation rate, the Cobb Mountain event was recorded in Holes 854B and 854C, and the Reunion event was recorded in Holes 854A and 854C (Fig. 17, Table 5), further testimony to the stability of the characteristic remanence.

Our interpretation of the zonation below the hiatus was constrained by the nannofossil stratigraphy, and we assigned the normal polarity chronozone immediately below the hiatus to the uppermost Miocene Subchron C3A-n1 (5.35–5.53 Ma). Thus, based on the adjacent reversal boundaries, which bracket the Mn-rich layer, the 0.9-m zone between the Gauss/Gilbert boundary and C3A-n1 (t) encompasses 1.95 m.y., or an average sedimentation rate of 0.44 mcd/m.y. Additional constraints on the upper Miocene section include an estimated basement age of 9 Ma; this led to our assigning the normal polarity zone between 33 and 40 mcd to C4-n2, and identifying the upper part of C5-n1 at the bottom of the section. The resulting average sedimentation rate for the upper Miocene is 8.4 mcd/m.y.

Our interpretation of the upper Miocene section includes four normal polarity chronozones that do not appear in standard MPTS compilations (Fig. 17):

1. A reverse chronozone is associated with C3A-n3 (~26.5 mcd) and was recorded in both Holes 854B and 854C. A similar feature near C3A-n3 was also observed in Holes 844B, 845A, and 845B.

2. A normal chronozone was observed just above C4-n1 (at ~30 mcd) in both Holes 854B and 854C. A similar feature also occurs at Holes 852B, 852C, and 852D. Alternatively, we might interpret this as being a short reverse interval within C4-n1, as we did in Holes 845A, 853B, 853C, and 853D.

3. In Hole 854C, C4-n3 includes a reverse polarity chronozone at ~41.5 mcd. In Hole 854B, the equivalent segment is uninterpretable in the top of Core 138-854B-5H or is within the overlying core gap.

4. In both Holes 854B and 854C, a normal polarity chronozone was observed between C4A-n1 and C4A-n2 at ~45.9 mcd. A similar feature was also identified in Holes 845B, 848C, and 848D.

Clearly, our interpretation of additional subchronozones for the upper Miocene at Site 854 needs confirmation from shore-based studies of discrete samples. Moreover, possible implications of these chronozones to MPTS developments will depend on their identification at other geographical areas to ascertain their global character.

## SEDIMENTATION RATES

A sedimentary section just over 50 m thick covering the time interval from the late Pleistocene to the bottom of the late Miocene was recovered at Site 854. Biostratigraphic age control was somewhat reduced at Site 854, but sufficient constraint was provided by nannofossils and radiolarians to ensure that the excellent magnetostratigraphic record was properly interpreted.

The composite depth section for Site 854 is given in Table 6. This composite was formed by comparing shipboard measurements of GRAPE, magnetic susceptibility, and percentage of reflectance (from the automated color analyzer) at adjacent holes. These comparisons were then integrated to form a single composite depth section for the

Table 5. Reversal boundary depths from Site 854.

Core, section interval (cm)	Depth (mbsf)	Depth (mcd)	Interpretation	Age (Ma)	Comments
138-854A-1H-2, 115	2.65	4.10		0.73	
1H-3, 98	3.98	5.43	Jaramillo (t)	0.91	
1H-4, 0	4.50	5.95	Jaramillo (o)	0.98	Section break
1H-7, 58	9.58	11.03	Olduvai (t)	1.66	
2H-1, 60	10.50	11.55	Olduvai (o)	1.88	
2H-2, 52	11.92	12.97	Reunion (t)	2.06	
2H-2, 62	12.02	13.07	Reunion (o)	2.09	
2H-4, 88	15.28	16.33	M/G	2.47	
2H-5, 62	16.52	17.57	Kaena (t)	2.92	
2H-5, 78	16.68	17.73	Kaena (o)	2.99	
2H-5, 92	16.82	17.87	Mammoth (t)	3.08	
2H-5, 112	17.02	18.07	Mammoth (o)	3.18	
2H-6, 60	18.00	19.05	G/G	3.40	
2H-6, 148	18.88	19.93	C3A-n1 (t)	5.35	
138-854B-1H-3, 108	4.08	4.08	B/M	0.53	
1H-4, 82	5.32	5.32	Jaramillo (t)	0.91	
1H-4, 130	5.80	5.80	Jaramillo (o)	0.98	
1H-5, 45	6.45	6.45	Cobb (t)	1.10	Midpoint
1H-5, 55	6.55	6.55	Cobb (o)	1.10	Midpoint
2H-2, 40	10.30	10.60	Olduvai (t)	1.66	
2H-2, 128	11.18	11.48	Olduvai (o)	1.88	
2H-5, 118	15.58	15.88	M/G	2.47	
2H-6, 72	16.62	16.92	Kaena (t)	2.92	
2H-6, 88	16.78	17.08	Kaena (o)	2.99	
2H-6, 98	16.88	17.18	Mammoth (t)	3.08	
2H-6, 118	17.08	17.38	Mammoth (o)	3.18	
3H-1, 88	18.78	21.13	C3A-n1 (o)	5.53	
3H-2, 18	19.58	21.93	C3A-n2 (t)	5.68	
3H-2, 138	20.78	23.13	C3A-n2 (o)	5.89	
3H-4, 52	22.92	25.27	C3A-n3 (t)	6.37	
3H-5, 20	24.10	26.45	R-gtN		
3H-5, 68	24.58	26.93	N-gtR		
3H-5, 132	25.22	27.57	C3A-n3 (o)	6.50	
3H-7, 52	27.42	29.77	N-gtR		
4H-2, 115	30.05	32.65	C4-n1 (o)	6.78	
4H-3, 30	30.70	33.30	C4-n2 (t)	6.85	
5H-2, 142	39.82	43.67	C4A-n1 (t)	7.90	
5H-3, 148	41.38	45.23	C4A-n1 (o)	8.21	Section break
5H-4, 58	41.98	45.83	blip (t)		
5H-4, 78	42.18	46.02	blip (o)		
5H-4, 128	42.68	46.53	C4A-n2 (t)	8.41	
5H-5, 58	43.48	47.33	C4A-n2 (o)	8.50	
5H-6, 22	44.62	48.47	C4A-n3 (t)	8.71	
5H-6, 68	45.08	48.93	C4A-n3 (o)	8.80	
5H-6, 98	45.38	49.23	C5-n1 (t)	8.92	
138-854C-2H-1, 95	4.55	5.35	Jaramillo (t)	0.91	
2H-1, 142	5.02	5.82	Jaramillo (o)	0.98	
2H-2, 60	5.70	6.50	Cobb (t)	1.10	Midpoint
2H-2, 72	5.82	6.62	Cobb (o)	1.10	Midpoint
2H-5, 22	9.82	10.62	Olduvai (t)	1.66	
2H-5, 108	10.68	11.48	Olduvai (o)	1.88	
2H-6, 82	11.92	12.72	Reunion (t)	2.06	
2H-6, 88	11.98	12.78	Reunion (o)	2.09	
3H-2, 8	14.68	16.68	M/G	2.47	
3H-2, 108	15.68	17.68	Kaena (t)	2.92	
3H-2, 122	15.82	17.68	Kaena (o)	2.99	
3H-2, 135	15.95	17.95	Mammoth (t)	3.08	
3H-3, 5	16.15	18.15	Mammoth (o)	3.18	
3H-3, 98	17.08	19.08	G/G	3.40	
3H-4, 32	17.93	19.93	C3A-n1 (t)	5.35	
3H-4, 150	19.11	21.11	C3A-n1 (o)	5.53	Section break
3H-5, 80	19.91	21.91	C3A-n2 (t)	5.68	
3H-6, 42	21.03	23.03	C3A-n2 (o)	5.89	
4H-1, 98	23.58	26.28	R-gtN		
4H-1, 142	24.02	26.72	N-gtR		
4H-2, 60	24.70	27.40	C3A-n3 (o)	6.50	
4H-3, 142	27.02	29.72	N-gtR		
4H-4, 52	27.62	30.32	R-gtN		
4H-4, 92	28.02	30.72	C4-n1 (t)	6.70	
4H-5, 138	29.99	32.69	C4-n1 (o)	6.78	
4H-6, 42	30.53	33.23	C4-n2 (t)	6.85	
5H-3, 98	36.08	39.78	C4-n2 (o)	7.28	
5H-4, 75	37.35	41.05	C4-n3 (t)	7.35	
5H-4, 102	37.62	41.32	R-gtN		
5H-4, 145	38.05	41.75	N-gtR		
5H-5, 50	38.60	42.30	C4-n3 (o)	7.41	
5H-5, 48	40.08	43.78	C4A-n1 (t)	7.90	
5H-7, 60	41.70	45.40	C4A-n1 (o)	8.21	
6H-1, 92	42.52	41.73	N-gtR		
6H-2, 5	43.15	42.35	C4-n3 (o)	7.41	Section break
6H-3, 2	44.62	43.82	C4A-n1 (t)	7.90	Section break
6H-3, 140	46.00	45.20	C4A-n1 (o)	8.21	
6H-4, 42	46.52	45.72	N-gtR		
6H-4, 78	46.88	46.08	R-gtN		
6H-4, 125	47.35	46.55	C4A-n2 (t)	8.50	
6H-6, 55	49.65	48.85	C4A-n3 (t)	8.71	
6H-6, 118	50.28	49.48	C4A-n3 (o)	8.80	
6H-7, 0	50.60	49.80	C5-n1 (t)	8.92	Section break

B/M = Brunhes/Matuyama; M/G = Matuyama/Gauss; G/G = Gauss/Gilbert. t = termination; o = onset.

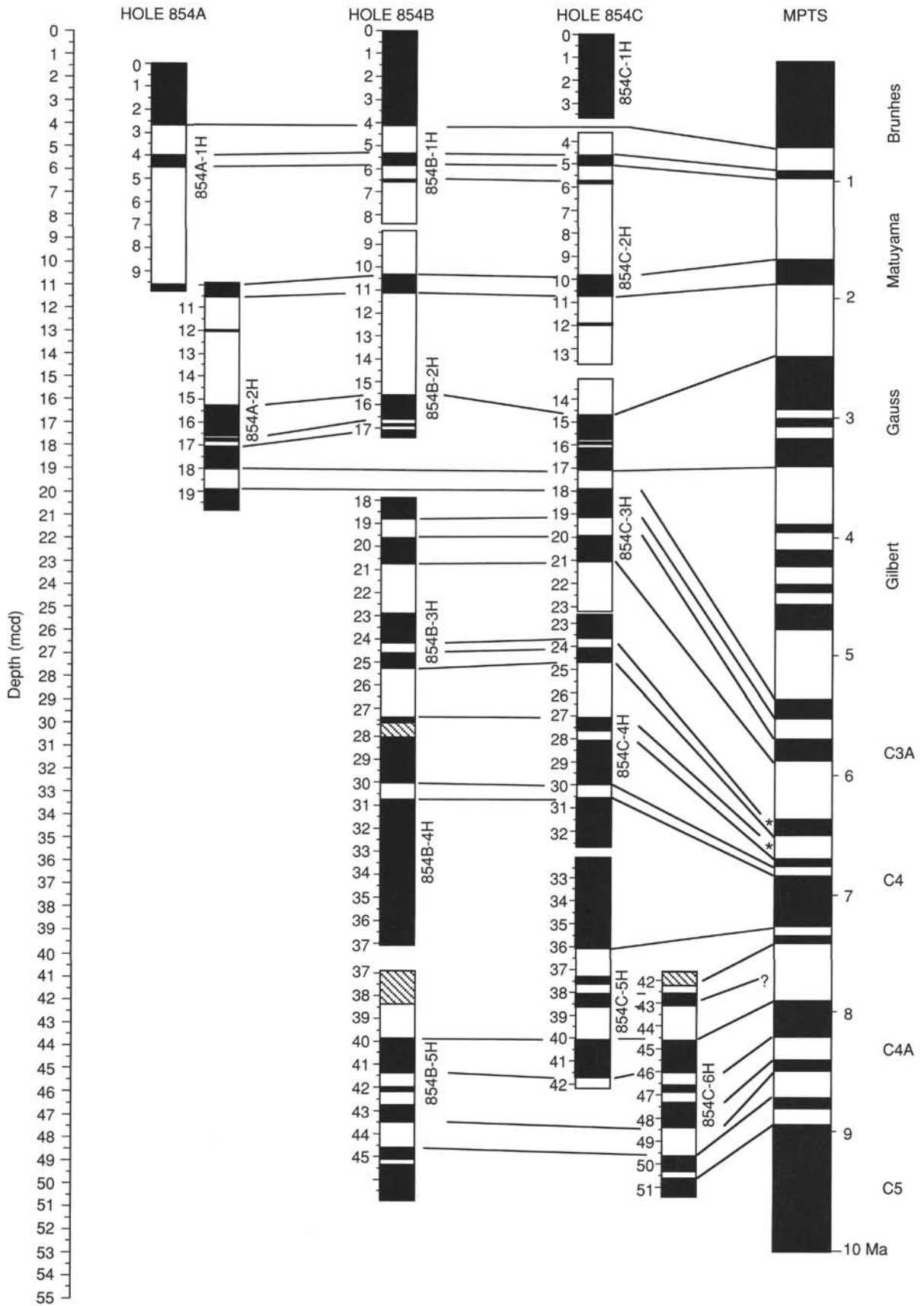


Figure 17. Magnetostratigraphic synthesis at Site 854. Depth ticks on individual cores are in meters below seafloor (mbsf). Cores are located at appropriate composite depth (mcd). Black zones = normal polarity; white zones = reverse polarity; hatched zones are not interpreted. MPTS = magnetic polarity time scale.

**Table 6. Depths of top and bottom of each core in Site 854 in the composite depth section.**

Core no.	Depth (mbsf)	Length (m)	Composite depth (mcd)	Delta (m)
138-854A-1H	0–9.96	9.96	1.45–11.41	1.45
138-854A-2H	9.90–19.87	9.97	10.95–20.92	1.05
138-854A-3X	19.40–20.36	0.96	20.65–21.61	1.25
138-854B-1H	0–8.38	8.38	0–8.38	0
138-854B-2H	8.40–18.04	9.64	8.70–18.34	0.30
138-854B-3H	17.90–27.95	10.05	20.25–30.30	2.35
138-854B-4H	27.40–37.35	9.95	30.00–39.95	2.60
138-854B-5H	36.90–46.89	9.99	40.75–50.74	3.85
138-854C-1H	0–3.60	3.60	0.15–3.75	0.15
138-854C-2H	3.60–13.72	10.12	4.40–14.52	0.80
138-854C-3H	13.10–23.12	10.02	15.10–25.12	2.00
138-854C-4H	22.60–32.67	10.07	25.30–35.37	2.70
138-854C-5H	32.10–42.23	10.13	35.80–45.93	3.70
138-854C-6H	41.60–51.71	10.11	40.80–50.91	–0.80

site (a detailed discussion on the construction of composite sections during Leg 138 is presented in Hagelberg et al., this volume).

For the holes and cores listed in Column 1 of Table 6, Column 2 gives the ODP sub-bottom depth of the core top and bottom in meters below seafloor (mbsf). Note that the depth given in Column 2 corresponds to the depth of the bottom of the recovered core. This depth places the core catchers in their correct position in the composite depth section and is not the same as the standard ODP core-catcher depth. Column 3 shows the length of core recovered. Column 4 gives the composite depth of the core top and bottom in meters composite depth (mcd). Column 5 indicates the amount of offset between the ODP depth and the composite depth. Conversion from ODP sub-bottom to composite depths can be done by adding the offset listed in Column 5 for a given core.

The magnetic susceptibility record at Site 854 has high amplitudes and variability throughout the section, while both the GRAPE and percentage of reflectance records were of low amplitude in many intervals. Consequently, the susceptibility record was the primary data set used to form a composite section for this site (Fig. 18, back-pocket). For the three holes drilled at Site 854 (3 cores in Hole 854A, 5 cores in Hole 854B, and 6 cores in Hole 854C), overlap was maintained throughout the sequence. This section was shorter here than at any of the other Leg 138 sites (50.91 mcd), and sedimentation rates are lowest (see below). In the first two cores, distortion between overlapping sections was noticeable. The last core in Hole 854C, Core 138-854C-6H, was taken with only a 4.5-m advance to avoid hitting basement with the APC, so that only a short (4 m) core of undisturbed material was anticipated. However, a full 10 m of cored material was recovered. The upper 4.5 m of this core overlapped completely with the bottom of the previous core, 138-854C-5H (Fig. 18, back-pocket) and was undisturbed, providing clear magnetostratigraphy. The drill pipe must have moved laterally between successive cores.

The sedimentation rate record for Site 854 was based entirely on the clear paleomagnetic record from the Brunhes down to C5-n1 (older than 8.92 Ma). Down to ~20 mcd, both nannofossils and radiolarians provided sufficient time control to control the magnetostratigraphic sequence absolutely. Nannofossil data confirm the presence of a hiatus at ~19.5 mcd; Sample 138-854A-2H-6, 100 cm, was assigned to Zone CN12 (younger than 3.56 Ma), while Sample 138-854A-2H-7, 60 cm, was assigned to Zone CN9b (older than 4.98 Ma).

In the section between 20 and 40 mcd, only intermittent samples contained nannofossils. Sample 138-854C-6H-1, 140 cm (42.2 mcd) contains *Discoaster berggreni*, showing it to be no older than ~7.5 Ma. Below this depth, the samples are barren of nannofossils, but the number of magnetic reversals detected can only be reasonably explained by postulating a significant change to a lower sedimentation rate at a little below 42 mcd. Table 7 gives the control points selected to generate the plots of age vs. depth shown in Figure 19, where the depth ranges within which the datums for the nannofossils

and radiolarians were observed are shown. In Table 7, all the control points are magnetic reversals; the mean depth (mcd) of each was used, except for the top of the Olduvai at 11.03 mcd in Hole 854A; this depth is significantly different from depths in Holes 854B and 854C because of core distortion that is evident in Figure 18 (back-pocket).

The pattern of sedimentation rate variation vs. age (Fig. 20) and depth (Fig. 21) shows a sedimentation rate of 0.23 m/m.y. (or a hiatus) through the interval from 3.5 to 5.3 Ma that encompasses the time of

**Table 7. Control points for sedimentation rates.**

Composite depth (mcd)	Sedimentation rate (m/m.y.)	Age (Ma)	Remarks
0	5.6	0	Top of sedimentary section
4.09	7.11	0.73	B. Brunhes Chron
5.37	7.0	0.91	T. Jaramillo Subchron
5.86	5.83	0.98	B. Jaramillo Subchron
6.56	7.23	1.1	Cobb Mountain
10.61	4.05	1.66	T. Olduvai Subchron
11.5	8.24	1.88	B. Olduvai Subchron
16.36	2.29	2.47	B. Matuyama Chron
17.39	1.57	2.92	T. Kaena Subchron
17.5	1.78	2.99	B. Kaena Subchron
17.66	2.0	3.08	T. Mammoth Subchron
17.86	5.5	3.18	B. Mammoth Subchron
19.0	5.37	3.4	B. Gauss Chron
19.5	0.23	3.5	Extrapolated
19.93	6.61	5.35	T. C3A-n1
21.12	5.33	5.53	B. C3A-n1
21.92	5.52	5.68	T. C3A-n2
23.08	4.56	5.89	B. C3A-n2
25.27	17.08	6.37	T. C3A-n3
27.49	16.15	6.5	B. C3A-n3
30.72	17.0	6.7	T. C4-n1
33.27	15.14	6.85	B. C4-n1
39.78	18.14	7.28	B. C4-n2
41.05	20.83	7.35	T. C4-n3
42.3	2.92	7.41	B. C4-n3
43.73	5.13	7.9	T. C4A-n1
45.32	6.1	8.21	B. C4A-n1
46.54	10.33	8.41	T. C4A-n2
47.47		8.5	B. C4A-n2
48.66	5.67	8.71	T. C4A-n3
49.21	6.11	8.8	B. C4A-n3
49.52	2.58	8.92	T. C5-n1

T = top; B = bottom.

highest sedimentation rate in most Leg 138 sites. The interval of highest sedimentation rate, between 6.3 and 7.4 Ma, precedes the high sedimentation rate interval in the other Leg 138 sites. Thus, this site may show the effect, whereby at times of increased productivity along the equator (which depresses the equatorial CCD), the CCD to the north moved upward.

## INORGANIC GEOCHEMISTRY

Five interstitial water samples were taken from Site 854, all in Hole 854B (Table 8). The first two samples came from Sections 2 and 5 of the first core, at 3.0 and 7.5 mbsf, respectively. One sediment sample was collected for pore water from every core to the basement, beginning with Core 138-854B-2H. Problems with squeezing prevented us from collecting a water sample from Core 138-854B-3H.

Core 138-854B-1H consists of clayey foraminifer nannofossil ooze. This sediment also contains 5% to 10% oxides (see "Lithostratigraphy" section, this chapter). Core 138-854B-2H is composed of the same dominant lithology. The oxide content increases dramatically in Core 138-854B-3H, where the sediments grade into very dark brown oxide clay, with up to 11% manganese oxides. Oxide clays persist through Core 138-854B-4H. The last core in this hole, Core 138-854B-5H, begins as a light yellowish-brown nannofossil clay, but grades into a black metalliferous clay and clayey metalliferous sediment, becoming progressively more oxide-rich toward the bottom (see "Lithostratigraphy" section, this chapter).

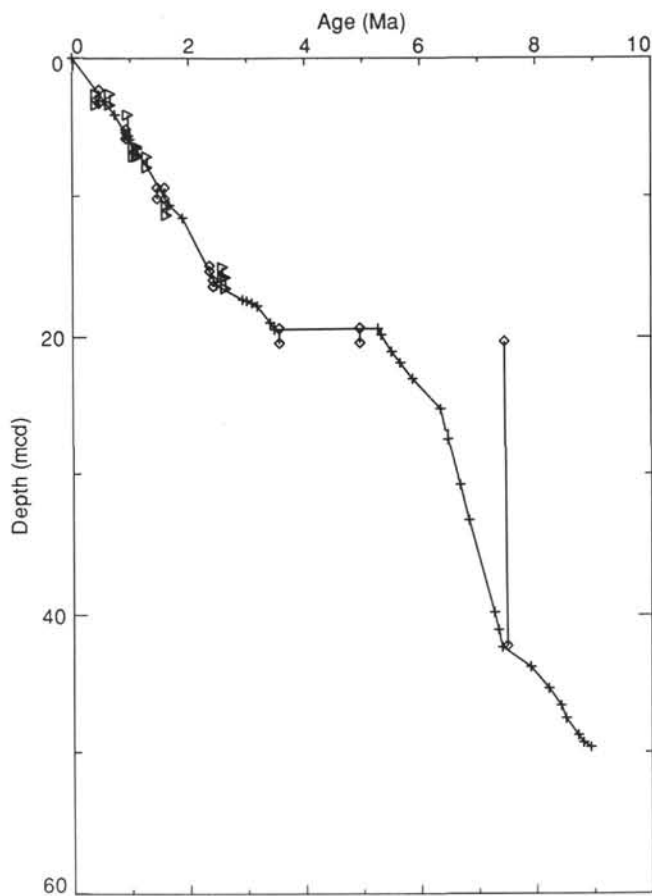


Figure 19. Plot of age vs. depth for Site 854 based on the calibration points in Table 7, compared with the nanfossil (diamond) and radiolarian (triangle) datums. Age control points from Table 7 are indicated by crosses. For each datum, the depth limits within which it was observed are indicated; where only a single symbol is visible the limits were too close to indicate at this plot scale.

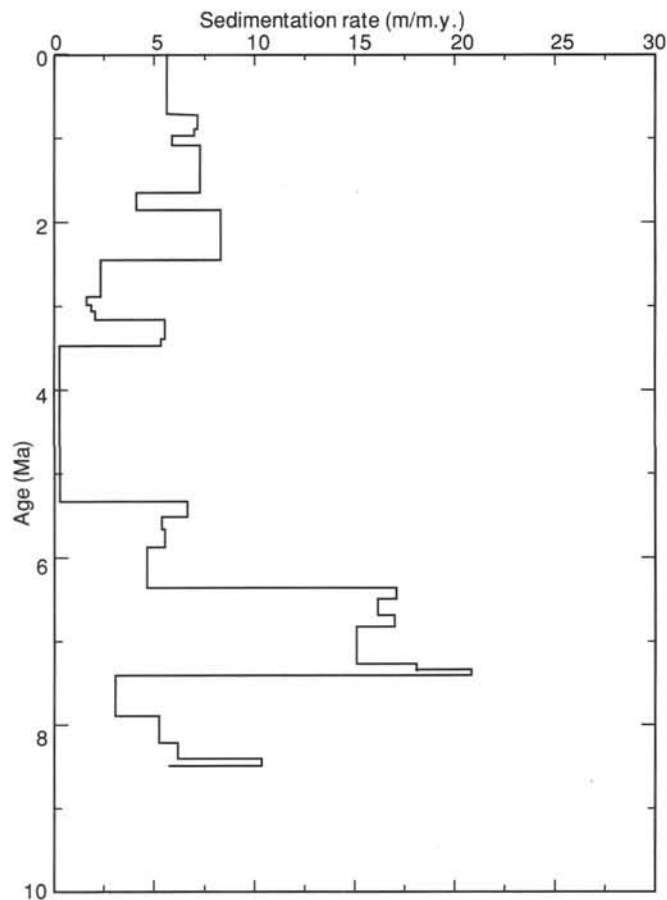


Figure 20. Linear sedimentation rate vs. age based on data in Table 7.

In general, sediments in Hole 854B consist of oxide-rich and clayey nanfossil oozes. Clays and oxides at Site 854 are even more prominent than at Site 853.

As at Sites 852 and 853, the smell of H<sub>2</sub>S was completely absent at Site 854, and ammonia levels were <10 μM (Table 8). By analogy with these sites, one would expect that the sediments at Site 854 might be oxidizing throughout. This prediction is borne out by the chemistry of the pore waters (Table 8) and is also consistent with the low sedimentation rates (see "Sedimentation Rates" section, this chapter) and low organic carbon contents (see "Organic Geochemistry" section, this chapter) reported for this site.

The total spread in interstitial sodium (Fig. 22A) and chloride (Fig. 22B) concentrations at this site is 0.7% and 0.8%, respectively. These variations are within the uncertainties of these measurements.

The greatest alkalinity at Site 854 (a modest 2.932 mM) occurs in the uppermost sample (Fig. 22C). This profile is similar to the one at Site 853 and suggests that early diagenesis has been confined to the sediment/water interface, where oxygen and nitrate have been consumed to oxidize organic matter (Froelich et al., 1979). Early diagenesis produces pore waters having alkalinities slightly higher than in bottom water (Fig. 22C), without consuming sulfate (Fig. 22D). Slow burial of organic carbon generates alkalinity near the sediment/water interface, which allows for an effective exchange with bottom water, thus keeping the pore water more oxidizing.

Data from this leg demonstrate that pore waters of slowly accumulating sediments tend to be less corrosive and that this situation has a direct impact on the degree of recrystallization within the sediment column (e.g., see Fig. 32, "Site 851" chapter, this volume). On the other hand, microfossils deposited in slowly accumulating sediments were exposed to bottom water for longer periods of time, increasing the risk of dissolution.

The sulfate profile at Site 854 (Fig. 22D) is unique for this leg because it shows sulfate increasing with depth. The total range in

Table 8. Interstitial-water geochemical data for Hole 854B.

Core, section, interval (cm)	Depth (mbsf)	pH	Salinity	Chloride (mM)	Sodium (mM)	Alkalinity (mM)	Sulfate (mM)	Magnesium (mM)	Calcium (mM)	Potassium (mM)	Strontium (μM)	Lithium (μM)	Silica (μM)	Ammonia (μM)
138-854B-1H-2, 145-150	3.0	7.48	35.5	558	480	2.932	28.23	52.59	10.44	11.5	88	26.1	525	<10
138-854B-1H-5, 145-150	7.5	7.47	35.0	557	478	2.627	28.42	52.49	10.95	11.7	90	26.0	790	<10
138-854B-2H-6, 145-150	17.4	7.54	—	360	479	2.544	28.61	53.01	11.71	11.0	88	24.8	486	<10
138-854B-4H-6, 145-150	36.4	7.43	36.3	361	479	2.352	29.07	53.01	13.16	10.7	90	24.6	385	<10
138-854B-5H-6, 145-150	45.9	7.42	—	559	476	2.511	29.16	52.76	13.89	10.2	88	24.9	374	<10

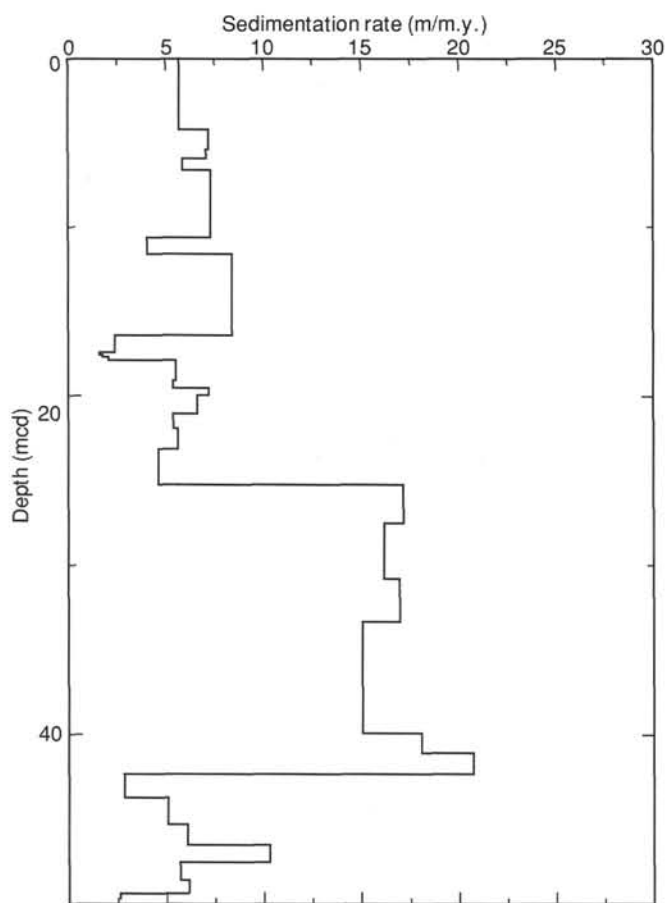


Figure 21. Linear sedimentation rate vs. composite depth based on data in Table 7.

sulfate is only 3.2% relative, but the trend is consistent downhole. Sulfate does not normally increase with depth in marine pore waters, except those associated with evaporites (McDuff et al., 1978). If real, this trend may indicate oxidation of basaltic sulfur and diffusion into the sediment column.

Because sulfate is not being reduced at this site, one might not expect to see the decreasing magnesium and calcium concentrations associated with calcium carbonate precipitation (Baker, 1986; Suess et al., 1988; Pedersen and Shimmiel, 1991). Magnesium (Fig. 23A) values are consistent in this way, as they remain invariant throughout the sediment column.

Calcium (Fig. 23B) values increase linearly with depth. This profile is indicative of low-temperature weathering of basalt and diffusive communication with the sediment column (McDuff, 1981). Crustal alteration also is indicated by decreasing potassium (Fig. 23C).

Interstitial silica levels at this site (Fig. 23D) are similar to those at the previous site. This profile is not easily explained because it does not seem to be predicted by reactions for the known sources or sinks for silica in deep-sea sediments. The observation that these silica levels are relatively low for deep-sea sediment pore waters probably reflects the low abundance of siliceous microfossils at this site (see "Biostratigraphy" section, this chapter).

Also similar to the situation at Site 853 is the result that strontium does not show a clear maximum at depth (Fig. 24B). This finding supports the earlier conclusion (see "Inorganic Geochemistry" section, "Site 851" chapter, this volume) that the amount of strontium released during recrystallization is directly related to the corrosiveness of the pore waters, and thus to the extent of diagenesis. Clearly, the burial rate of organic carbon at this site is so low that early

diagenesis occurred very near the interface, which allowed most of the corrosive character produced by oxidation of organic matter to escape to bottom water before burial. The most direct indication of this "equilibration" process is pH; the range in pH at Site 852 is 7.09 to 7.22, while it is 7.42 to 7.54 at this site (Table 8).

Interestingly, lithium concentrations do not change with depth at this site (Fig. 24A). This result suggests that the lithium removal observed at every Leg 138 site before Site 853 is somehow associated with recrystallization, as inferred from its mirror-image relationship with strontium.

In summary, alkalinity and sulfate profiles suggest that early diagenesis at Site 854 was confined to degradation reactions by oxygen and nitrate very near or at the interface. The highest alkalinity occurs at the top of the hole, indicating a relatively low organic carbon burial rate, as do nearly constant sulfate concentrations. Crystallization was not operative at this site, leading to limited variations in magnesium, calcium, lithium, and strontium.

## ORGANIC GEOCHEMISTRY

### Carbonate and Organic Carbon

Inorganic carbon was measured in Hole 854B following the methods outlined in the "Explanatory Notes" chapter (this volume). From the inorganic carbon data, we calculated the weight percent of calcium carbonate (%CaCO<sub>3</sub>). The analytical results are listed in Table 9 (CD ROM, back pocket) with respect to both ODP depth (mbsf) and to composite depth (mcd; see "Sedimentation Rates" section, this chapter). If a duplicate analysis was performed on a given sample, the mean value of the original analysis and the duplicate is listed in Table 9 (CD ROM, back pocket). Duplicate percentage of CaCO<sub>3</sub> analyses are listed in Table 10. The results indicate a reproducibility of 1.0%.

Figures 25 and 26 show percentages of CaCO<sub>3</sub> at Site 854 vs. ODP depth and vs. composite depth and age, respectively, based on datum levels identified at Site 854 (see "Sedimentation Rates" and "Paleomagnetism" sections, this chapter). In the uppermost 26 m, the percentage of CaCO<sub>3</sub> record at Site 854 varies between 20% and 70%. At 26 mbsf, values decrease to 0% CaCO<sub>3</sub>. Between 30 and 40 mbsf, carbonate values rise to a maximum of 54%. From 40 mbsf to the end of the recovered section, the CaCO<sub>3</sub> values are 0%. Sedimentation rates between 3.5 and 5.35 Ma were extremely low (see "Sedimentation Rates" section, this chapter), perhaps indicating a hiatus.

### Accumulation Rates

The accumulation rates of bulk-sediment (bulk MAR), CaCO<sub>3</sub> MAR, and noncarbonate MAR are listed in Table 11 and plotted vs. composite depth in Figure 27 and vs. age in Figure 28. The accumulation rate of bulk sediment was significantly lower than at any of the previous equatorial sites. Instead of the characteristic and well-defined patterns in CaCO<sub>3</sub> MAR that characterized the bulk-sediment MARs at each of the previous sites, variability in bulk MARs at Site 854 was derived from noncarbonate accumulation maxima between 6 and 7.5 Ma, possibly related to hydrothermal processes. In this interval, the accumulation rate of noncarbonate MAR is approximately twice the value reached during the late Pliocene and Pleistocene.

### Gas Geochemistry

One sample for gas analysis was taken from each core of Hole 854B. We measured no hydrocarbon gas above detection limits.

## PHYSICAL PROPERTIES

### Introduction

Physical properties were routinely measured in cores from Site 854. For whole-round sections, GRAPE density, compressional-wave

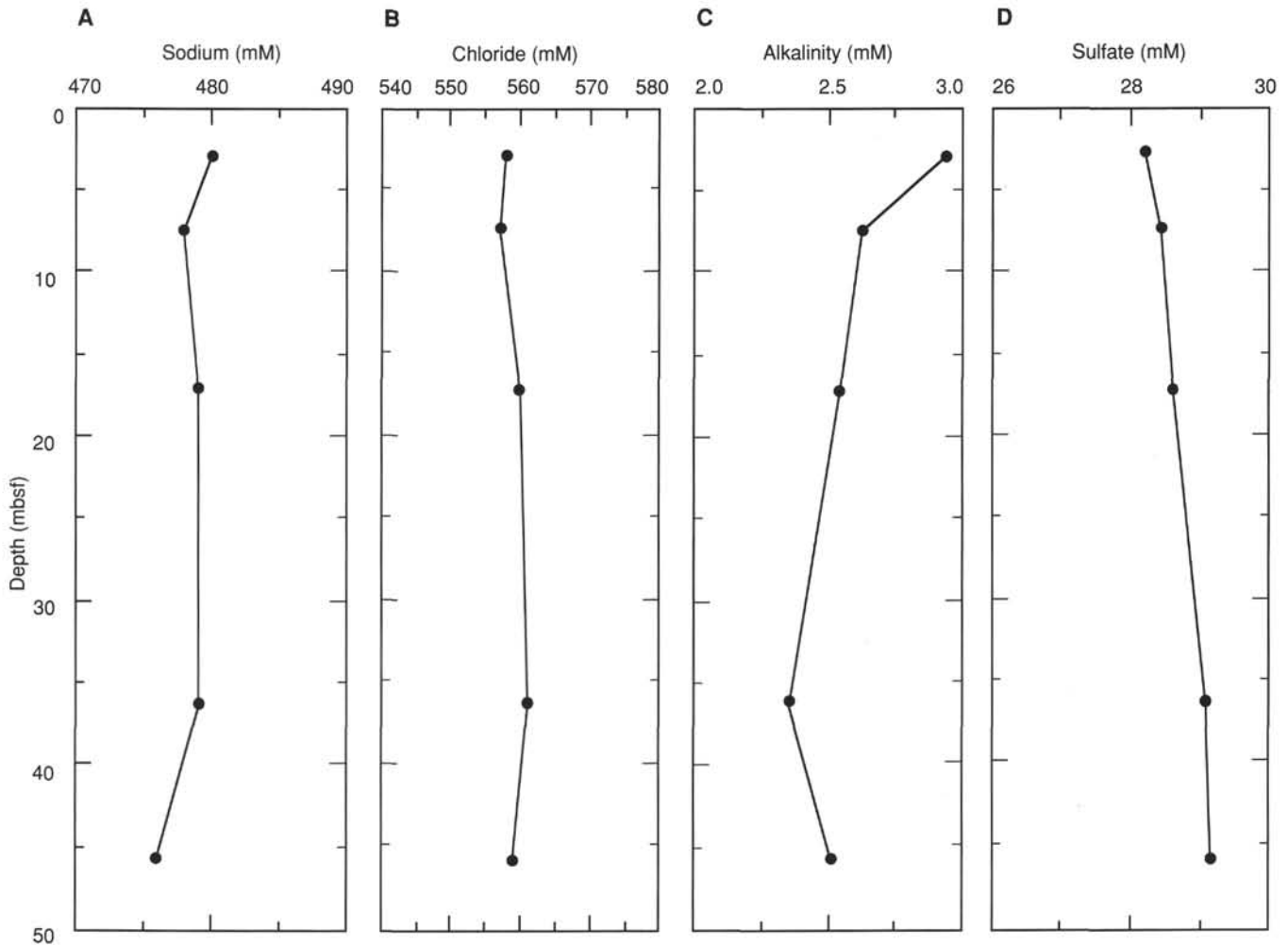


Figure 22. Interstitial-water geochemical data vs. depths (mbsf) for Hole 854B. A. Sodium. B. Chloride. C. Alkalinity. D. Sulfate.

velocity (using the multisensor track, MST), and thermal conductivity were measured. Wet-bulk density, dry-bulk density, grain density, porosity, wet water content, dry water content, and void ratio, vane shear strength, and compressional-wave velocity were measured in split cores. Although velocity was measured using the digital sonic velocimeter (DSV), the data were not stored because of a computer storage problem.

Physical properties were measured in every section of cores recovered from Hole 854B. Shear strength and index properties were analyzed twice per section. In Hole 854C, index properties were measured only once per section. Shear strength and thermal conductivity were not measured in Hole 854C. Index property samples were always taken at the same depth interval as the velocity measurements.

Thermal conductivity was routinely measured for Sections 1, 3, and 5 of each core in Hole 854B.

### Index Properties

Wet-bulk density ranges from 1.17 to 1.36 g/cm<sup>3</sup> (Fig. 29; Table 12, CD ROM, back pocket), water contents from 154% to 446% (Fig. 30), and porosity from 79% to 92% (Fig. 31). No obvious trend with depth is apparent in these profiles. Grain density varies between 1.98 to 2.92 g/cm<sup>3</sup>, with most values lying in the range between 2.40 and 2.90 g/cm<sup>3</sup> (Fig. 32). Lithologic variation may account for downhole variation in the index property profiles (see discussion below).

Table 10. Duplicate analyses of percentage of CaCO<sub>3</sub> in samples from Site 854.

Core, section, interval (cm)	ODP depth (mbsf)	Composite depth (mcd)	First run CaCO <sub>3</sub> (%)	Second run CaCO <sub>3</sub> (%)	Absolute value of CaCO <sub>3</sub> (difference)
138-854B-1H-1, 32-34	0.33	0.33	19.09	18.49	0.60
138-854B-1H-4, 34-36	4.85	4.85	19.46	19.77	0.31
138-854B-2H-1, 33-35	8.74	9.04	15.66	13.86	1.80
138-854B-2H-1, 102-104	9.43	9.73	46.19	48.95	2.76
138-854B-2H-6, 33-35	16.24	16.54	64.89	65.21	0.33
138-854B-3H-1, 102-104	18.93	21.28	53.21	52.55	0.67
138-854B-4H-6, 32-34	35.23	37.83	53.55	54.09	0.54
138-854B-4H-6, 102-104	35.93	38.53	16.33	17.03	0.70
Average					0.96

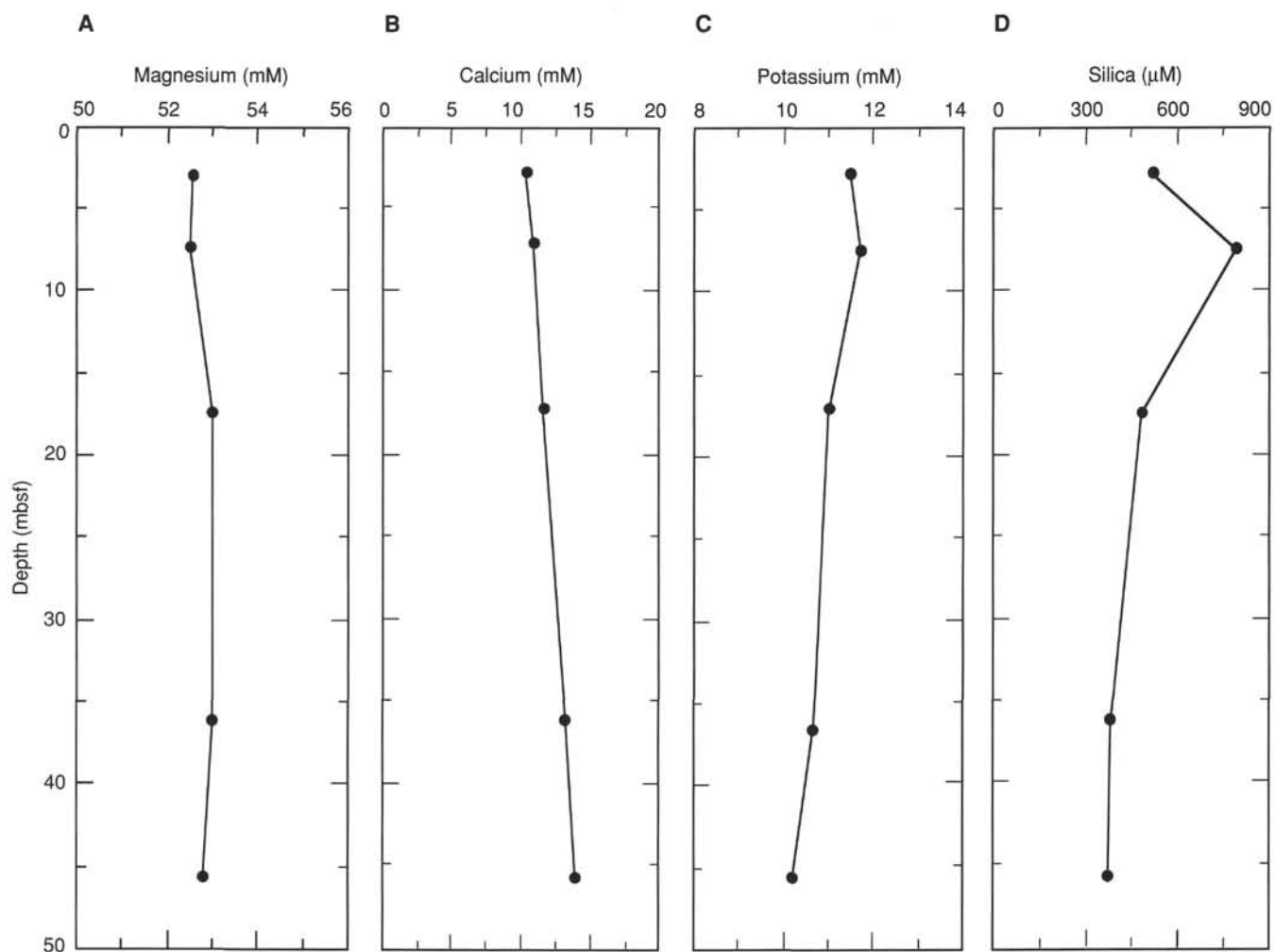


Figure 23. Interstitial-water geochemical data vs. depths (mbsf) for Hole 854B. **A.** Magnesium. **B.** Calcium. **C.** Potassium. **D.** Silica.

### Shear Strength

The profile of undrained shear strength for Hole 854B is presented in Figure 33 (Table 13, CD ROM, back pocket). No consistent trend with depth is seen in the profile. The shear strength data vary between 19 and 49 kPa, with most values between 30 and 38 kPa.

### Thermal Conductivity

Thermal conductivity (Fig. 34; Table 14, CD ROM, back pocket) varies from 0.74 to 1.00 W/(m • K). The mean value is 0.86 W/(m • K). Thermal conductivity decreases slightly between 20 and 40 mbsf, as a result of an increase in porosity over that interval and is constant with depth below 40 mbsf.

### Relationships of Physical Properties to Lithology

Variations in index properties at Site 854 are mainly controlled by sediment composition, especially by variations in carbonate, clay, and oxide content. The effect of composition on index properties can be seen by comparing calcium carbonate content (see "Organic Geochemistry" section, this chapter) and index properties profiles.

The occurrence of clay-rich zones at ~10 and 22–32 mbsf results in a decrease in wet-bulk density and an increase in dry water content and porosity. However, grain density is relatively constant in those intervals.

In the interval from 42 mbsf to basement, index properties

change rapidly, indicating a major change in sediment composition. The occurrence of clayey metalliferous sediment, consisting of high amounts of iron and manganese oxides, results in an abrupt decrease in grain density and porosity. The discrepancy in grain density between Holes 854B and 854C over this interval can be corrected by plotting the data vs. composite depth (see "Sedimentation Rates" section, this chapter).

### SUMMARY AND CONCLUSIONS

Site 854 is the northernmost site drilled along the western transect of Leg 138. Our primary objective for the site was to sample the region well north of the present position of the Intertropical Convergence Zone (ITCZ). This atmospheric boundary marks the dividing line between the Northern and Southern Hemisphere trade winds. Most sites drilled during Leg 138 are either within the southeast trade winds (Sites 846–851) or near the extreme positions of the ITCZ (Sites 852 and 853) and thus give either a Southern Hemisphere signal or a mixed signal of the ITCZ's movement in response to change in climate. The only other sites drilled during Leg 138 in a more northerly position (Sites 844 and 845) are close to the Central American continent and may contain terrigenous sediment transported by processes other than just eolian. Thus, Site 854 provides a unique record of eolian sediments transported by the Northern Hemisphere winds.

Site 854, as all other sites along the 110°W transect, is located ~900 km west of the East Pacific Rise on crust generated ~10 Ma.

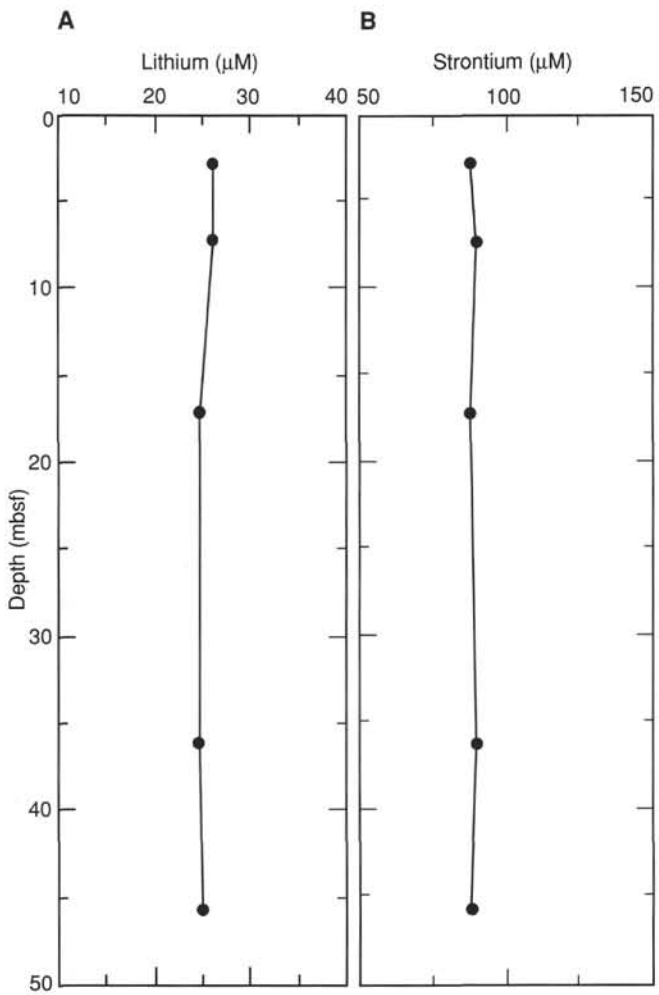


Figure 24. Interstitial-water geochemical data vs. depths (mbsf) for Hole 854B. A. Lithium. B. Strontium.

The backtracked path of the site is straightforward, constrained only by the movement of the Pacific Plate. Poles of rotation of the Pacific Plate have been estimated based on traces of hot spots (Duncan and Claque, 1985) and also by using the age distribution of sediments from DSDP sites along the equatorial sediment bulge (van Andel et al., 1975; see Fig. 2). While the backtracked paths for Site 854 differ, depending on which of these poles of rotation was used, neither of the reconstructions had Site 854 crossing under the equator.

The sediments at Site 854 reflect its more northerly position relative to other sites along the 110°W transect. The site is north of the dominant regions of divergence (at the equator and at the boundary between the NEC and NECC) and thus is not in a region of elevated surface productivity. This was reflected in the overall low sedimentation rates, which resulted in a section <50 m thick on crust equivalent in age to other sites along the transect.

The sediments in the younger part of the section are dominated by clay, nannofossils, and foraminifers. Siliceous microfossils are present, but in much lower abundances. Other indications of decreased productivity in the region can be seen in the interstitial-water chem-

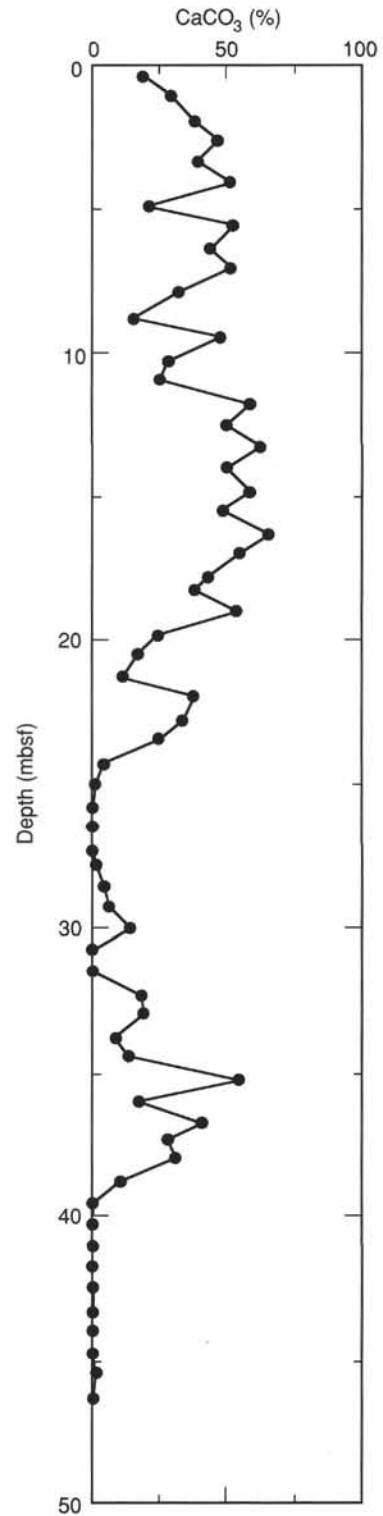


Figure 25. Downhole record of percentages of CaCO<sub>3</sub> vs. ODP depth (mbsf) for Site 854.



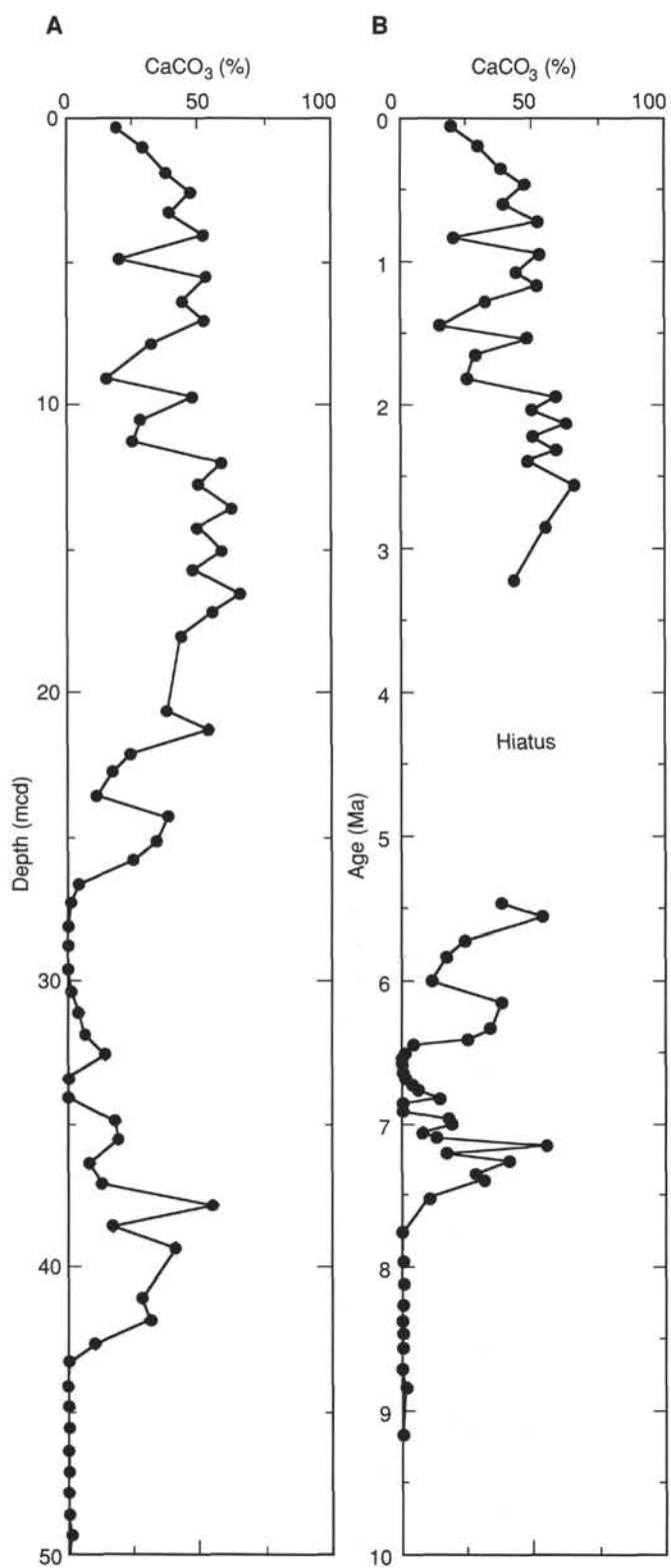


Figure 26. Plots of percentages of  $\text{CaCO}_3$  vs. composite depth (mcd) (A) and age (B) for Site 854.

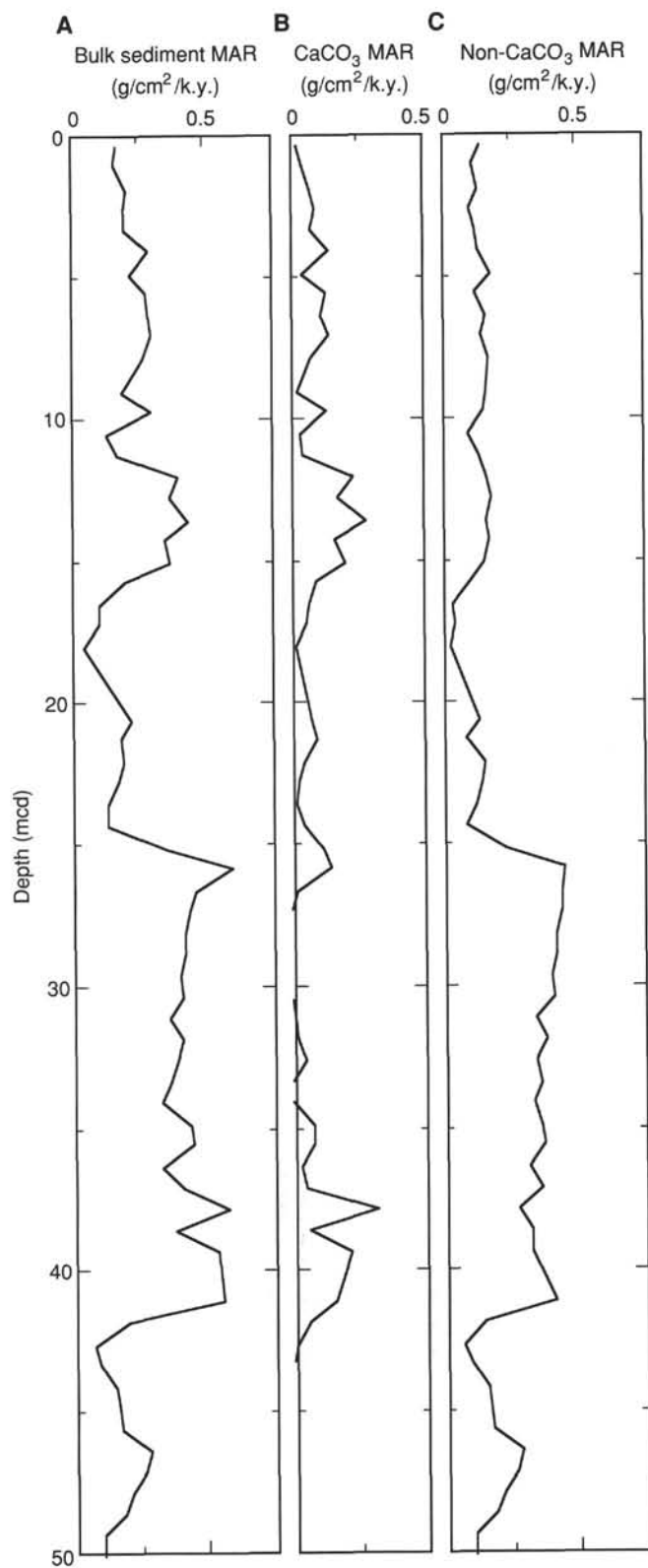


Figure 27. Mass accumulation rates of (A) bulk sediment, (B)  $\text{CaCO}_3$ , and (C) non- $\text{CaCO}_3$  vs. composite depth at Site 854. The line shows discrete accumulation rates calculated for each sample.

**Table 11. Averages values of sedimentary parameters calculated over time intervals defined by chronostratigraphic levels.**

Composite depth (mcd)	Age (Ma)	Mean CaCO <sub>3</sub> (%)	Sed. rate (m/m.y.)	Mean DBD (g/cm <sup>3</sup> )	Mean bulk MAR (g/cm <sup>2</sup> /k.y.)	Mean CaCO <sub>3</sub> MAR (g/cm <sup>2</sup> /k.y.)	Mean CaCO <sub>3</sub> MAR (g/cm <sup>2</sup> /k.y.)
4.09	0.73	36.59	5.60	0.37	0.21	0.08	0.13
5.37	0.91	19.61	7.11	0.33	0.23	0.05	0.19
5.86	0.98	51.69	7.00	0.44	0.31	0.16	0.15
6.56	1.10	42.89	5.83	0.43	0.25	0.11	0.14
10.61	1.66	34.40	7.23	0.36	0.26	0.09	0.17
11.50	1.88	24.70	4.05	0.30	0.12	0.03	0.09
16.36	2.47	54.05	8.24	0.46	0.38	0.20	0.17
17.39	2.92	59.68	2.29	0.49	0.11	0.07	0.05
17.50	2.99		1.57				
17.66	3.08		1.78				
17.86	3.18		2.00				
19.07	3.40	42.47	5.50	0.43	0.24	0.10	0.14
19.50	3.48		5.37				
19.50	5.29		0.00				
19.93	5.35		7.17				
21.12	5.53	37.39	6.61	0.36	0.24	0.09	0.15
21.92	5.68	52.88	5.33	0.36	0.19	0.10	0.09
23.08	5.89	20.13	5.52	0.37	0.20	0.04	0.16
25.27	6.37	27.10	4.56	0.32	0.15	0.04	0.11
27.49	6.50	9.42	17.08	0.30	0.51	0.05	0.46
30.72	6.70	0.25	16.15	0.26	0.41	0.00	0.41
33.27	6.85	7.78	17.00	0.23	0.39	0.03	0.36
39.78	7.28	18.60	15.14	0.28	0.42	0.08	0.34
41.05	7.35		18.14				
42.30	7.41	28.93	20.83	0.30	0.61	0.18	0.44
43.73	7.90	4.99	2.92	0.28	0.08	0.00	0.08
45.32	8.21	0.13	5.13	0.32	0.16	0.00	0.16
46.54	8.41	0.08	6.10	0.32	0.19	0.00	0.19
47.47	8.50	0.17	10.33	0.34	0.35	0.00	0.35
48.66	8.71	0.08	5.67	0.38			
49.21	8.80		6.11				
49.52	8.92	0.42	2.58	0.43	0.11	0.00	0.11

Note: After this table was constructed on board the ship, depths of the age control points were changed (see "Sedimentation Rates" section, this chapter, for the final selection of age control points). These depth changes were often minor (less than 5 m). None of these changes were incorporated in this table, nor in the accompanying figure. DBD = dry-bulk density; MAR = mass accumulation rate.

istry, which suggests that the sediment section has been oxic and that little diagenesis, driven by the decay of organic matter, has taken place within the sediment column. The high clay content combined with little or no diagenesis resulted in higher magnetic susceptibilities than have been seen at most sites along the western transect (Fig. 35B) and a stable magnetic remanence. The excellent magnetic stratigraphy obtained at the site allowed us to project a detailed picture of sedimentation history of this area over the past 9 m.y.

The first sediment to accumulate above the newly formed Site 854 was a black manganese- and iron-rich metalliferous clay. Accumulation was relatively low, starting at ~2.5 m/m.y (Fig. 35A). This metalliferous clay was unlike the other sediment intervals seen above

basement at other Leg 138 sites and reflects the general reduced surface production at this site, even during the Miocene. The backtracked position of this site, based on van Andel et al.'s (1975) rotation, was still at ~10°N at this time (Table 15), which should place it well north of the present-day region of high sedimentation. This unusual metalliferous sediment may reflect sedimentary influxes dominated both by ridge-crest processes and by processes of authigenic accumulation of manganese oxides, making the section a unique end-member of metal oxide accumulation.

For the most part, sedimentation rates between 7.5 and 8 Ma remained low at Site 854. After this time, rates increased by a factor of 3 to ~15 m/m.y. The early part of this interval of increased

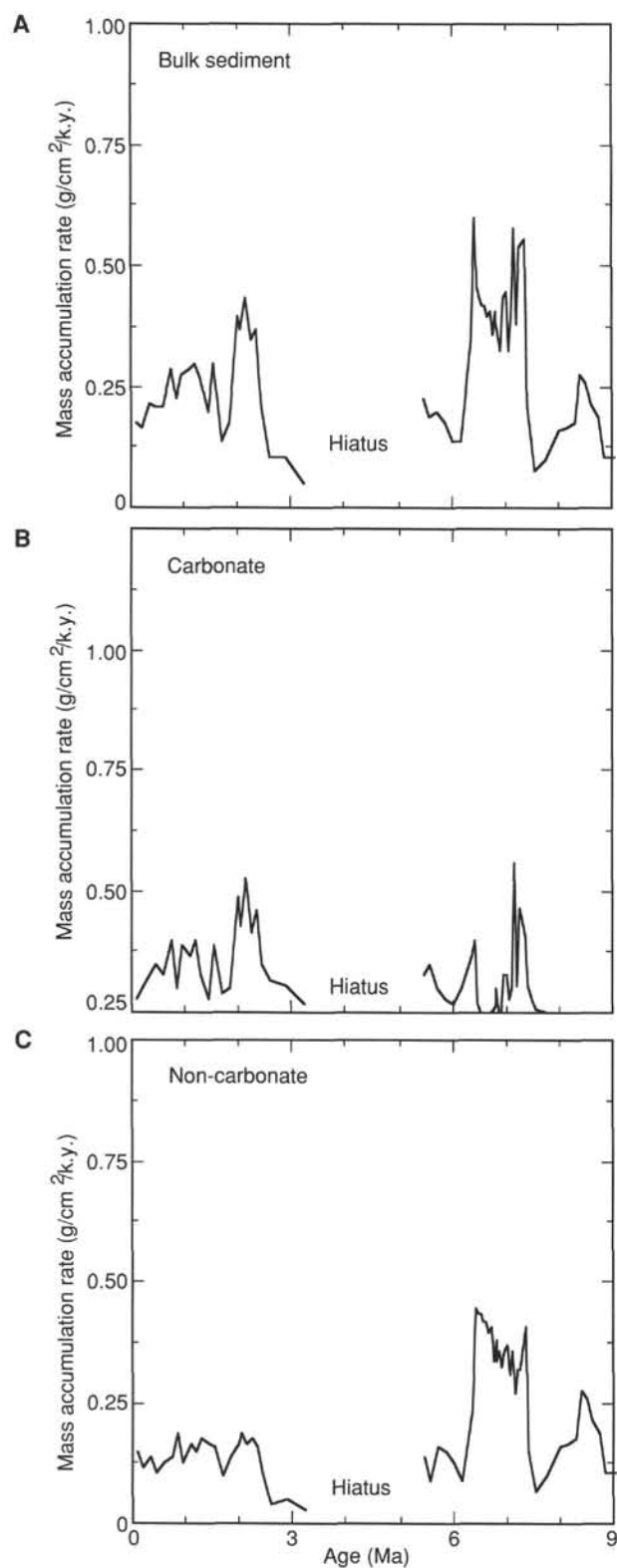


Figure 28. Mass accumulation rates of (A) bulk sediment, (B) CaCO<sub>3</sub>, and (C) non-CaCO<sub>3</sub> vs. age in sediments from Site 854. The line shows discrete accumulation rates calculated for each sample.

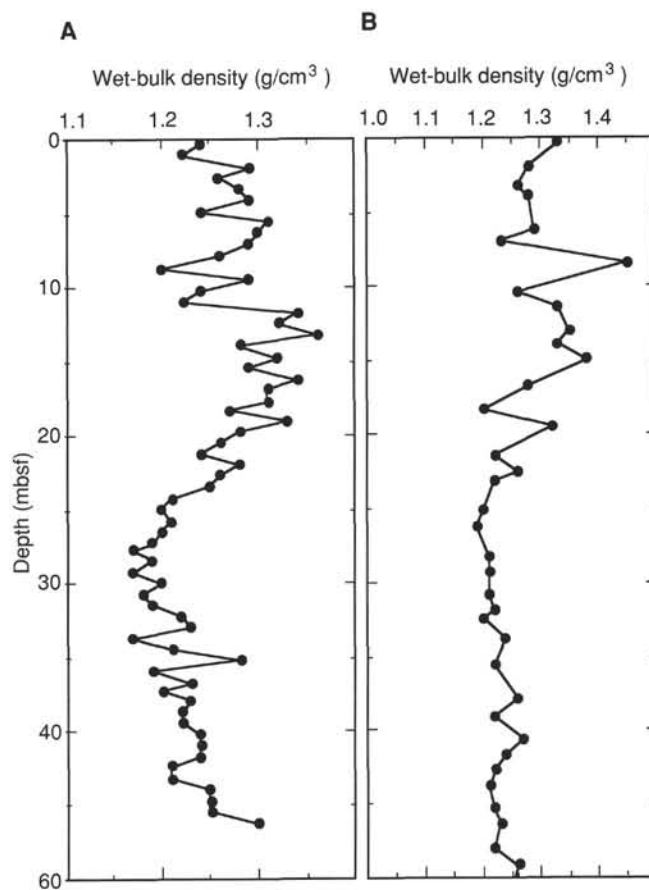


Figure 29. Plot of wet-bulk density vs. depth, Holes 854B (A) and 854C (B).

sedimentation rates has much higher abundances of calcium carbonate (Fig. 35C), with nanofossils being ~60% of the sediment (and sometimes as high as 80%). While this increase in carbonate accumulation may reflect a decrease in carbonate dissolution, the increase in sedimentation rate at 7.5 Ma occurred at a somewhat younger age than was seen at some of the other sites along the transect. Sites with magnetic stratigraphy seem to show some increases at this time, while sites with only biostratigraphic control do not sufficiently resolve sedimentation rate changes during this interval to determine if these differences are real. Future stratigraphic analyses will be critical for resolving such differences.

During the interval of high sedimentation, the sediments changed from a clayey nanofossil ooze to an oxide-rich clay between ~22 and 32 mbsf. Even with this lithologic change to reduced carbonate

Table 15. Backtracked path for Site 851.

Ma	Latitude (°N)	Longitude (°W)
1	10.95	108.78
2	10.70	108.05
3	10.46	107.33
4	10.22	106.60
5	9.98	105.88
6	9.75	105.15
7	9.51	104.43
8	9.28	103.70
9	9.06	102.98

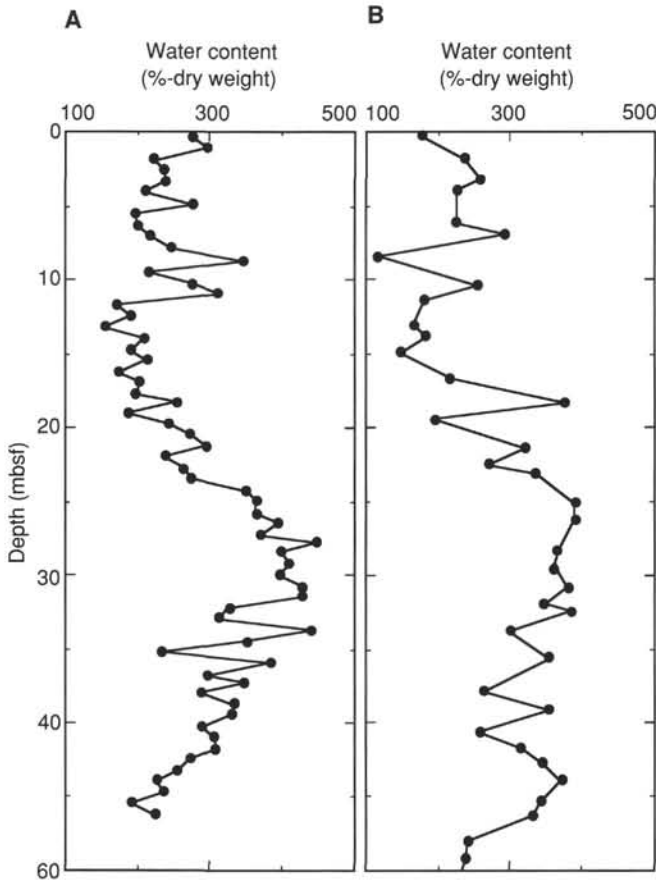


Figure 30. Water content (%-dry weight) vs. depth, Holes 854B (A) and 854C (B).

content, sedimentation rates remained at the 15 m/m.y. level. Noncarbonate mass accumulation rates showed a maximum between 6 and ~7.5 Ma (see Fig. 28), while carbonate accumulation rates were high only in the interval from 7 to ~7.5 Ma. The absence of siliceous microfossils in these sediments suggests that nonbiogenic accumulation must have been significantly higher at this site during this time.

At ~6.3 Ma, sedimentation rates decrease to ~5 m/m.y. Biostratigraphic and lithostratigraphic evidence suggest that the interval between 3.5 and 5.3 Ma may be represented by a hiatus. Above this interval sedimentation rates are relatively low, averaging ~5 m/m.y. In this upper interval, siliceous microfossils and foraminifers are present, but only as minor components of the sediments.

The possible hiatus at Site 854 occurs at a time when elevated sedimentation rates were observed at essentially all other sites along the 110°W transect. If this increase in general accumulation solely reflects a decrease in carbonate dissolution, we might expect an increase in carbonate accumulation at Site 854 as well. Piasias and Prell (1985) suggested, based on carbonate budget calculations from the equatorial Pacific Ocean, that the marked increase in rates, observed mostly at sites near the equator, reflected a narrowing of the productivity belt without a significant change in total carbonate being accumulated in the region. The data used by Piasias and Prell (1985) were that of van Andel et al. (1975), which were augmented by results from DSDP Leg 85. The more detailed stratigraphic framework

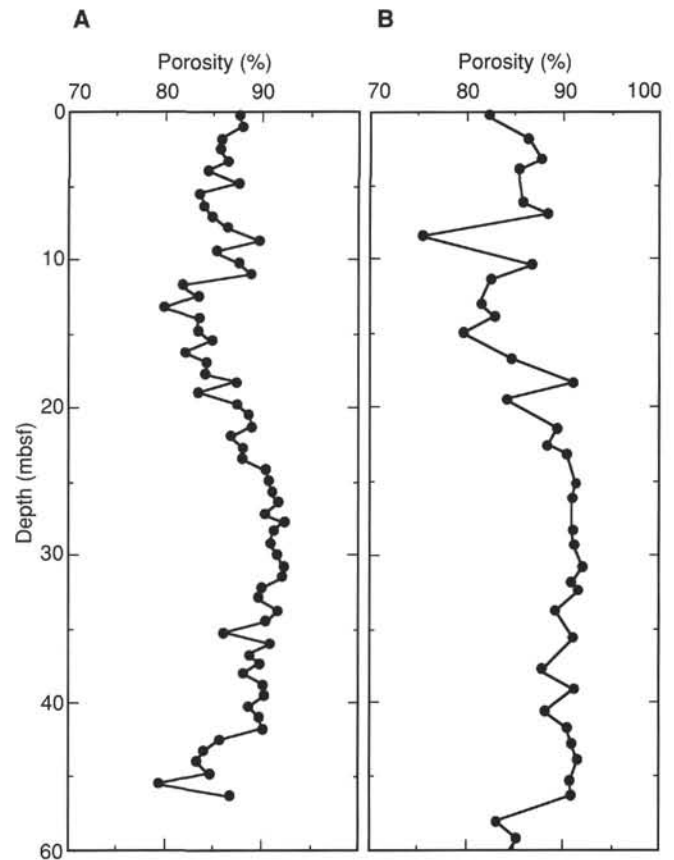


Figure 31. Porosity vs. depth, Holes 854B (A) and 854C (B).

possible for the Leg 138 transect should, one would hope, provide a more rigorous test of this hypothesis.

#### REFERENCES

- Baker, P. A., 1986. Pore water chemistry of carbonate-rich sediments, Lord Howe Rise, Southwest Pacific Ocean. In Kennett, J. P., von der Borch, C. C. et al., *Init. Repts. DSDP, 90*: Washington (U.S. Govt. Printing Office), 1249-1256.
- Duncan, R., and Clague, D., 1985. Pacific plate motion is recorded by linear volcanic chains. In Narin, A.E.M., Stehli, F. G., and Uyeda U. (Eds.), *Ocean Basins and Margins, Vol. 7A*: New York (Plenum Pubs.), 89-121.
- Froelich, P. N., Klinkhammer, G. P., Bender, M. L., Heath, G. R., Luedtke, N., Cullen, D., Dauphin, P., Hammond, D., Hartman, B., and Maynard, V., 1979. Early oxidation of organic matter in pelagic sediments of the Eastern Equatorial Atlantic: suboxic diagenesis. *Geochim. Cosmochim. Acta*, 43:1075-1090.
- Mammerickx, J., 1989. The Eastern Pacific Ocean and Hawaii. In Winterer, E. L., et al. (Eds.), *The Geology of North America*. Geol. Soc. Am., Plate 1C.
- McDuff, R. E., 1981. Major cation gradients in DSDP interstitial waters: the role of diffusive exchange between seawater and the upper ocean crust. *Geochim. Cosmochim. Acta*, 45:1705-1713.
- McDuff, R. E., Gieskes, J. M., and Lawrence, J. R., 1978. Interstitial water studies, Leg 42A. In Kidd, R. B., Worstell, P. J., et al., *Init. Repts. DSDP, 42*: Washington (U.S. Printing Office), 561-568.
- Pedersen, T. F., and Shimmiel, G. B., 1991. Interstitial water chemistry, Leg 117: contrasts with the Peru margin. In Prell, W. L., Niitsuma, N., et

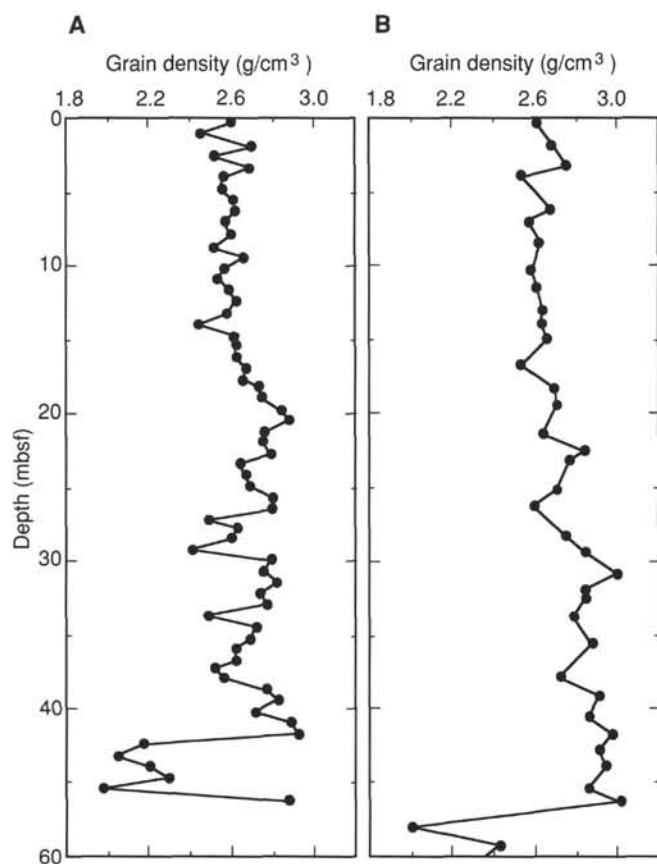


Figure 32. Grain density vs. depth, Holes 854B (A) and 854C (B).

al., *Proc. ODP. Sci. Results*, 117: College Station, TX (Ocean Drilling Program), 499-513.

Pisias, N. G., and Prell, W., 1985. Changes in calcium carbonate accumulation in the Equatorial Pacific during the late Cenozoic: evidence from HPC Site 572. In Sundquist, E. T., and Broecker, W. S. (Eds.), *The Carbon Cycle and Atmospheric CO<sub>2</sub>: Natural Variations Archean to Present*: Washington (Am. Geophys. Union), 443-454.

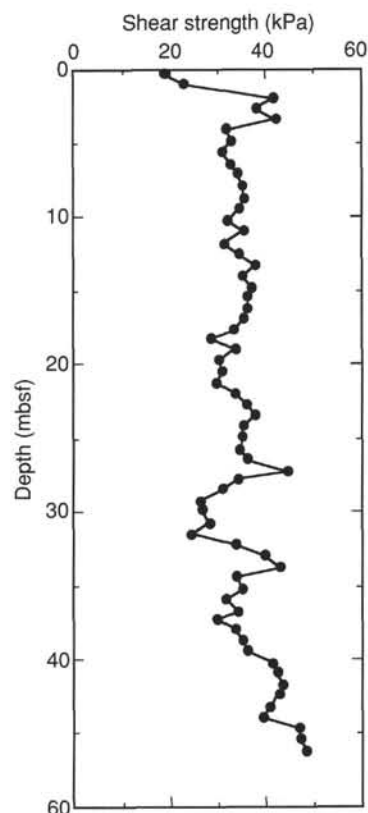


Figure 33. Undrained shear strength data for Hole 854B.

Suess, E., von Huene, Z. R., et al., 1988. *Proc. ODP. Init. Repts.*, 112: College Station, TX (Ocean Drilling Program).

van Andel, T. H., Heath, G. R., and Moore, T. C., 1975. Cenozoic tectonics, sedimentation, and paleoceanography of the central equatorial Pacific. *Geol. Soc. Am. Mem.*, 143.

Ms 138A-119

**NOTE: For all sites drilled, core description forms ("barrel sheets") and core photographs have been reproduced on coated paper and can be found in Section 8, beginning on page 1099. Forms containing smear-slide data can be found in Section 9, beginning on page 1435.**

**Formation microscanner images for this site are presented on microfiche in the back of Part 2.**

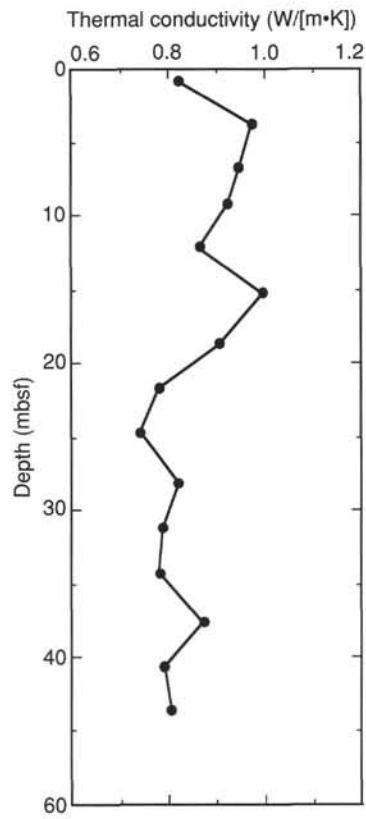


Figure 34. Thermal conductivity data for Hole 854B.

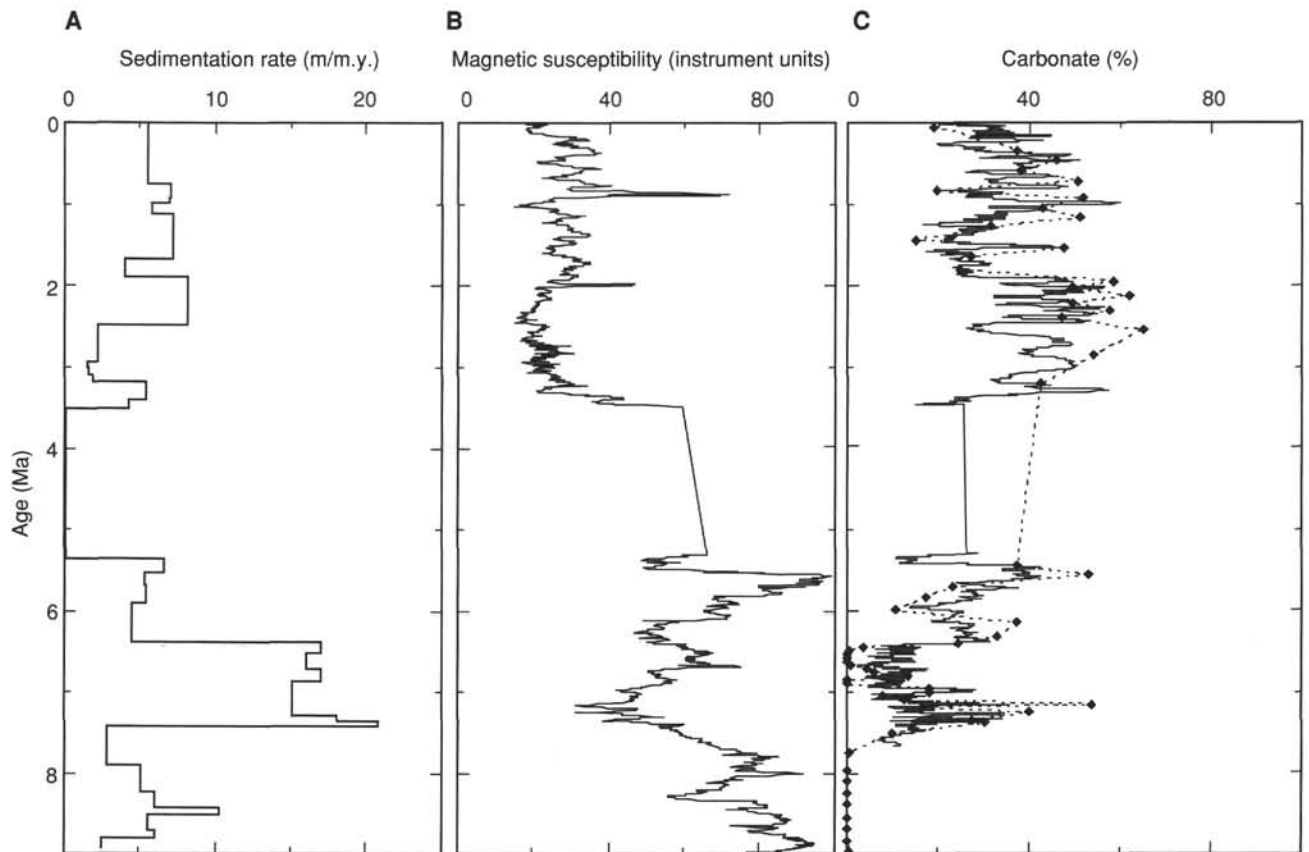


Figure 35. **A.** Sedimentation rate vs. sediment age. **B.** Magnetic susceptibility vs. age. **C.** Predicted (solid line) and measured carbonate content vs. age.